Monthly Notices
of the
ROYAL ASTRONOMICAL SOCIETY

MNRAS **478,** 2368–2387 (2018)
Advance Access publication 2018 May 14

doi:10.1093/mnras/sty1209

# Multiple populations within globular clusters in early-type galaxies exploring their effect on stellar initial mass function estimates

W. Chantereau,[★] C. Usher and N. Bastian

*Astrophysics Research Institute, Liverpool John Moores University, 146 Brownlow Hill, Liverpool L3 5RF, UK*

Accepted 2018 May 2. Received 2018 October 5; in original form 2017 March 31

## ABSTRACT

It is now well-established that most (if not all) ancient globular clusters host multiple populations that are characterized by distinct chemical features such as helium abundance variations along with N–C and Na–O anticorrelations, at fixed [Fe/H]. These very distinct chemical features are similar to what is found in the centres of the massive early-type galaxies and may influence measurements of the global properties of the galaxies. Additionally, recent results have suggested that *M*/*L* variations found in the centres of massive early-type galaxies might be due to a bottom-heavy stellar initial mass function. We present an analysis of the effects of globular cluster-like multiple populations on the integrated properties of early-type galaxies. In particular, we focus on spectral features in the integrated optical spectrum and the global mass-to-light ratio that have been used to infer variations in the stellar initial mass function. To achieve this, we develop appropriate stellar population synthesis models and take into account, for the first time, an initial-final mass relation which takes into consideration a varying He abundance. We conclude that while the multiple populations may be present in massive early-type galaxies, they are likely not responsible for the observed variations in the mass-to-light ratio and IMF-sensitive line strengths. Finally, we estimate the fraction of stars with multiple populations chemistry that come from disrupted globular clusters within massive ellipticals and find that they may explain some of the observed chemical patterns in the centres of these galaxies.

**Key words:** galaxies: abundances – galaxies: star clusters: general – galaxies: stellar content.

## 1 INTRODUCTION

Massive early-type galaxies (ETGs) have long been known to show non-solar abundance patterns (e.g. Worthey, Faber & Gonzalez 1992; Trager et al. 2000; Gallazzi et al. 2006) with the observed increase in [$\alpha$/Fe] with galaxy mass being interpreted as an inverse relationship between mass and star formation time-scale (e.g. Matteucci 1994; Thomas et al. 2005). More recent works (e.g. Graves & Schiavon 2008; Johansson, Thomas & Maraston 2012; Conroy, Graves & van Dokkum 2014; Worthey, Tang & Serven 2014) have allowed the abundances of a range of elements to be measured from integrated galaxy light and shown that the abundances of elements such as C, N, and Na also increase with galaxy mass.

However, several lines of evidence show that the stellar populations of massive ETGs are not as simple as expected for populations that formed in a relatively short burst. Many ETGs show brighter far-UV-luminosities than would be expected for an old, metal-rich stellar population (e.g. Code & Welch 1979; Burstein et al. 1988; Greggio & Renzini 1990; Dorman, O'Connell & Rood 1995; Brown et al. 1997; O'Connell 1999; Brown et al. 2000; Yi et al. 2011). The colours of this 'UV-upturn' are correlated to the stellar mass-to-light ratio (*M*/*L*) and mass of the host galaxy (Burstein et al. 1988; Greggio & Renzini 1990; O'Connell 1999; Donas et al. 2007; Dalessandro et al. 2012; Zaritsky, Gil de Paz & Bouquin 2015). Recent works have also shown interesting radial abundance gradients in the centres of at least some ETGs. van Dokkum et al. (2017) found strong positive [O/Fe] and negative [Na/Fe] radial gradients but no or weak age or heavier [$\alpha$/Fe] gradients in 6 ETGs while Sarzi et al. (2017) found a strong negative [Na/Fe] gradient in the centre of M87, in addition to the reported IMF variations. These abundance trends do not appear to be the result of a classical galactic chemical enrichment, such as $\alpha$-enhancement (see e.g. van Dokkum et al. 2017). Thus the origin of these gradients is still uncertain (Schiavon 2007).

Cappellari et al. (2012) found that *M*/*L* strongly varies in the *r* band among ETGs and is correlated to the galaxy's velocity dispersion. They interpreted this as an IMF variation towards a bottom-heavy distribution (low-mass dwarf stars) for the most massive ETGs (those with the highest velocity dispersion). Evidence for a bottom heavy IMF in the centre of galaxies also comes from

---

[★] E-mail: w.chantereau@ljmu.ac.uk

© 2018 The Author(s)
Published by Oxford University Press on behalf of the Royal Astronomical Society

Downloaded from https://academic.oup.com/mnras/article-abstract/478/2/2368/4995915
by Liverpool John Moores University user
on 10 July 2018

detailed studies of the spectra of massive ETGs (e.g. van Dokkum & Conroy 2010; Conroy & van Dokkum 2012b; La Barbera et al. 2017) where absorption lines distinctive of dwarf stars are stronger and absorption lines indicative of giant stars are weaker than in stellar population synthesis models with Milky Way-like IMFs. Interpretation of these observations of IMF-sensitive spectral features is complicated by their (strong) dependence on chemical abundance (e.g. Conroy & van Dokkum 2012a) in massive ETGs.

Meanwhile, thanks to advances in instrumentation including multiplexed high-resolution spectrographs and high-resolution optical and ultraviolet imaging from space, ground-breaking observations have shaken the long-standing paradigm of globular clusters (GCs) being composed of a simple stellar population (e.g. Catelan, Valcarce & Sweigart 2010; Gratton, Carretta & Bragaglia 2012; Charbonnel 2016). Photometric observations highlight a large variety of features in colour-magnitude diagrams not consistent with simple stellar populations (see e.g. Piotto 2009; Milone et al. 2017) while spectroscopic studies provide conspicuous evidence of significant star-to-star variations of the light elements abundances. It appears that there are (at least) two main stellar populations within GCs, the first (1P) consists of stars that show the same chemical abundance patterns as field stars (at a given [Fe/H]). The second population (2P) shows distinct patterns, namely enhanced He, N, Na, and Al accompanied by depletion of C, O, and sometimes Mg (e.g. Gratton et al. 2012). These abundance anomalies have been found in (nearly) all of the ancient GCs studied to date, including extremely metal-poor and metal-rich (near solar) GCs in the Milky Way and nearby galaxies (e.g. Bastian & Lardo 2017).

GCs are mainly composed of a monometallic (i.e. they lack spreads in heavy elements such as Fe and Ca) and a coeval population of stars, therefore these abundance variations are not expected to be the results of standard stellar or galactic chemical evolution. These observed chemical features are rather thought to be the direct signatures of hydrogen-burning at high temperature, a process that is not at work in main sequence low-mass stars displaying these peculiar chemical patterns (Denisenkov & Denisenkova 1990). However, the origin of the abundance variations, or even if they are limited to GCs, is currently unknown (see the recent review by Bastian & Lardo 2017). We note that MPs are observed in massive star clusters as young as 2 Gyr (Martocchia et al. 2018) and in GCs with near solar metallicities (Tang et al. 2017; Schiavon et al. 2017b), showing that MP requires neither special conditions in the early universe nor low metallicities.

There are recent hints that the presence of MPs may not be a phenomenon restricted to GCs. For instance, a small fraction (∼2 per cent) of field stars in the halo and the inner Galaxy bear chemical features typical of these MPs. (Spiesman 1992; Carretta et al. 2010; Martell & Grebel 2010; Ramírez, Meléndez & Chanamé 2012; Martell et al. 2016; Schiavon et al. 2017a). At galactic scales, Strader et al. (2013) found an ultra-compact dwarf thought to be the stripped core of a galaxy enhanced in N and Na that could indicate the presence of similar self-enrichment to what is present in GCs. The chemical composition of MPs, especially the He-enhancement, has a great impact on their stellar evolution. Thus the presence of these He-rich stars has important effects on the observed properties of GCs (e.g. D'Antona, Caloi & Ventura 2010; Cassisi et al. 2014; Chantereau, Charbonnel & Meynet 2016; Charbonnel & Chantereau 2016; Tailo et al. 2016), hence it is timely to develop studies on their effects on galactic scales with appropriate stellar population synthesis models.

The peculiar chemical features observed in massive ETGs at a given age and metallicity (Na and N enhancement; Schiavon 2007; Conroy et al. 2014; van Dokkum et al. 2017, and O-depletion to a certain extent, van Dokkum et al. 2017) are reminiscent of the MP chemical patterns found in GCs. Parallels can also be drawn between the UV-upturn in ETGs and the bright UV luminosities of GCs with hot horizontal branches due to He enhanced stars. In addition, at a given age and metallicity, He-rich stars of MPs are less massive, have different luminosities, and display larger final masses than their He-normal counterpart. Thus, we might expect the He-rich population to have a different *M*/*L* than the chemically 'normal' population. It would then be interesting to investigate the integrated properties of MPs, and investigate if He-rich stars of GCs would be a viable alternative explanation for the observed *M*/*L* and spectral index variations between galaxies.

As the origin of the multiple population phenomenon is currently unknown, there are two possible mechanisms for which they might appear in massive early-type galaxies. The first is that the chemically peculiar stars are formed in GCs which are subsequently disrupted due to the tidal field of the host galaxy. The second is that multiple populations are not limited to GCs and can form within galaxies under specific conditions (i.e. high stellar densities or pressures). In the present work we explore the former option. We note that massive early-type galaxies posses populous GC systems (e.g. Harris, Harris & Alessi 2013) and that their GC systems display broad metallicity distributions with substantial numbers of GCs at solar and higher metallicity (e.g. Peng et al. 2006; Usher et al. 2012). Note also that our current understanding of star formation indicates that intense star formation (high metallicity) is accompanied by the formation of GCs (Kruijssen 2015; Pfeffer et al. 2017).

The goals of this paper are twofold. First, we explore the extent to which disrupted GCs are expected to contribute to the stellar populations of massive ETGs. For this we exploit recent advances in our understanding of star/cluster formation within galaxies as well as how the stellar population properties (i.e. the extent of MPs within them) depend on the cluster properties (i.e. mass). Secondly, we explore the effects of the peculiar abundance pattern of MPs (i.e. enhanced He, N, Na, Al, and depleted C and O) on the integrated properties of the populations, focusing on the *M*/*L* ratio, UV flux, and spectral indices. To do this, we create tailored integrated light stellar population models with MPs and compare them to both other models in the literature as well as to selected observations of ETGs. The underlying question motivating the current work is to what extent the observed MP phenomenon can explain the observed features of massive ETGs.

This paper is organized as follows. In Section 2 we investigate the fraction of second-population stars from GCs that might contribute to the peculiar abundance patterns observed in the core of ETGs. Then in Section 3, we present the initial-final mass relations and the stellar population synthesis models adapted to the MPs framework. In Section 4 we investigate the effects of the typical initial chemical compositions of MPs, initial mass functions, and ages on the resulting *M*/*L*. We present the effects of MPs on the spectral indices in Section 5 and we investigate their effect in the central regions of ETGs (Section 6). We finally discuss and summarize the results in Sections 7 and 8, respectively.

## 2 CONTRIBUTION TO THE FIELD OF DISRUPTED GLOBULAR CLUSTERS

We do not know if MPs can form directly within ETGs as their formation mechanism within GCs (and elsewhere) is currently unknown. However, disrupting GCs are expected to contribute heavily to the stellar populations in the central regions of ETGs since intense

Downloaded from https://academic.oup.com/mnras/article-abstract/478/2/2368/4995915
by Liverpool John Moores University user
on 10 July 2018

star formation leads to the formation of large numbers of massive star clusters (e.g. Whitmore et al. 1999; Bastian 2008; Kruijssen 2014) and since the tidal fields in the centres of massive galaxies effectively disrupt star clusters (e.g. Goudfrooij et al. 2004; Pfeffer et al. 2017). In this section we estimate the contribution of disrupted GCs to the field of the core of ETGs. The basic question that we hope to address later in the paper with this toy model is whether disrupted GCs could potentially be the origin of the 'anomalous chemistry' seen in ETGs.

For the initial estimate we assume that all formed GCs in the ETGs core have been disrupted, which agrees with the depressed numbers of GCs seen projected near the centres of ETGs relative to the outer regions of ETGs (e.g. McLaughlin 1999; Forbes et al. 2006; Peng et al. 2008). For the GC mass function, we adopt a power law with index of −2 and an upper limit of $10^8$ $M_\odot$, comparable to the most massive observed young massive clusters (e.g. Maraston et al. 2004; Bastian et al. 2006). While there is evidence for an environmentally dependent upper mass truncations (e.g. Gieles et al. 2006; Larsen 2009; Bastian et al. 2012; Johnson et al. 2017), we expect a high upper limit in the extreme high pressure environments in the inner regions of ETGs and do not expect much variations from galaxy to galaxy. Similarly, we expect the cluster formation efficiency ($\Gamma$) to be relatively high in such high pressure environments (e.g. Kruijssen 2015; Pfeffer et al. 2017), between 0.5 and 1, meaning that half to all stars form in clusters. Though in our toy model we assume all stars have the same age and metallicity, we would expect the age and metallicity distribution of stars that formed in GCs in the centres of ETGs to mirror that of field stars.

Recent surveys have found that the fraction of second population stars (enriched stars, $F_{\rm enriched}$) with GCs increases with increasing cluster mass ranging from ∼50 per cent at $10^5$ $M_\odot$ to near 85 per cent at $10^6$ $M_\odot$ (Milone et al. 2017). We use these measurements and an initial-current GC mass relationship (fig. 7, Kruijssen 2015) to derive a linear relation (in logarithmic mass) between initial cluster mass and enriched fraction between a faction of 0 at $1.7 \times 10^5$ $M_\odot$ and 1 at $3.2 \times 10^6$ $M_\odot$. Below an initial mass of $1.7 \times 10^5$ $M_\odot$ we set the fraction to 0; above $3.2 \times 10^6$ $M_\odot$ to 1. Note that unlike some MP formation scenarios we do not adopt extreme mass loss of the young GCs, i.e. that they were 10–30× more massive than at present.

Adopting a lower cluster mass limit of $10^2$ $M_\odot$, the fraction of enriched stars in the central regions of ETGs is then given by

$$F_{\rm ETG,enriched} = \frac{\Gamma}{M_{\rm total}} \times \int_{10^2}^{10^8} M^{-2} \times F_{\rm enriched}(M){\rm d}M. \qquad (1)$$

Adopting $\Gamma = 0.75$ and the Milone et al. (2017) relation for the relation between the fraction of enriched stars and the initial cluster mass results in an estimate of $F_{\rm ETG,\,enriched} = 0.35$, i.e. a third of the stars in the central regions of ETGs are expected to show the anomalous chemistry observed in GCs. However, not only does the enriched fraction vary with cluster mass, the *degree* of enrichment is also a function of cluster mass, with higher mass clusters hosting larger spreads in He, Na, and N (Carretta et al. 2010; Schiavon et al. 2013; Milone 2015; Milone et al. 2017). In the majority of GCs, however, most of the stars do not display the extreme abundances. If we use NGC 2808 as a test case, ∼13 per cent of the stars in this cluster belong to the extreme population, i.e. that with the largest He variations ($\Delta Y = 0.15$),[1] and a further 15 per cent of the stars are mildly enriched ($\Delta Y = 0.07$) with the rest not showing an appreciable variation in He. To estimate the possible He spread in ETGs due to disrupted clusters, we use the relation of Milone (2015) between cluster mass and the maximum He spread ($f_{\rm max,\,\Delta Y}$) and then distribute the stars in a similar way as in NGC 2808 with 13 per cent having the maximum $\Delta Y$, 15 per cent half the maximum $\Delta Y$, and the rest having $\Delta Y = 0$.

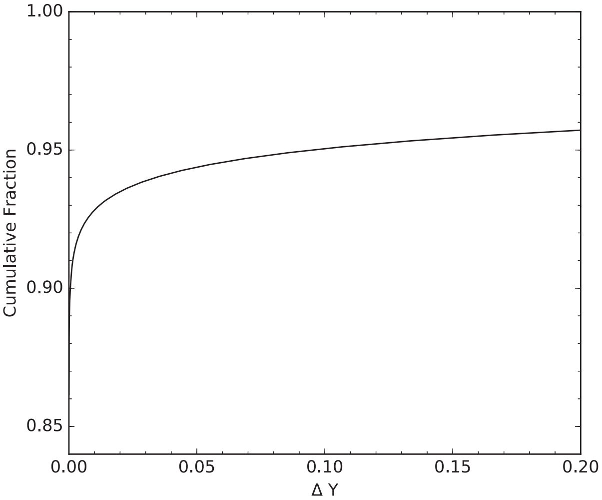

**Figure 1.** Cumulative fraction of helium spread ($\Delta Y$) for our ETG model. The fraction is based on the relation between GC luminosity and He spread of Milone (2015) and the assumption that 13 per cent of the stars have the maximum $\Delta Y$, 15 per cent have half the maximum $\Delta Y$, and the rest have $\Delta Y = 0$ together with the cluster mass function in equation (1).

The resulting distribution of $\Delta Y$ is shown in Fig. 1. For the given set of assumptions, we find that 93 per cent of the stars of the galaxy would be expected to have $\Delta Y < 0.01$ and 95 per cent of the stars have $\Delta Y < 0.07$. However, there is a relatively extended tail with 5 per cent of the stars having $\Delta Y > 0.1$. We note that our calculations are sensitive to the maximum initial GC mass, the initial-current GC mass relationship, and the assumption that present-day fraction of second-population stars is the same as at formation.

In summary, we find that disrupted GCs may contribute a substantial amount (∼35 per cent) of stars with second-population chemistry (enriched in N and Na while depleted in C and O) to the field population in the centres of ETGs. Disrupted GCs also contribute a small but significant fraction (∼5 per cent) of strongly He-enhanced stars.

## 3 STELLAR POPULATION SYNTHESIS MODELS

In this section we describe the stellar population synthesis models and initial-final mass relations used in this work. We emphasize that our models are intended to study the qualitative effects of He enhancement and of the CNONa abundance patterns present in GCs and are not constructed to fully reproduce the observed spectral energy distributions of GCs or galaxies. In the Appendix we compare our models to those of Conroy & van Dokkum (2012a) as well

---

[1] We use the He content as a discriminant between the multiple populations as it is the element that has the largest impact on the evolution of these stellar populations.

Downloaded from https://academic.oup.com/mnras/article-abstract/478/2/2368/4995915
by Liverpool John Moores University user
on 10 July 2018

as observed spectra of metal-rich GCs in the Milky Way and find qualitative agreement. We calculated stellar population synthesis models for a solar He content ($Y_{\rm ini}$= 0.26, also referred as He-normal content at $Z_{\odot}$) and for an enhanced He content ($Y_{\rm ini}$= 0.4) at solar metallicity and an age of 12.6 Gyr (typical ETG age and metallicity; e.g. Gallazzi et al. 2005; Conroy & van Dokkum 2012b; Conroy et al. 2014). We kept the metallicity mass fraction constant ($Z$= 0.0134; Asplund et al. 2009) between the solar He and He-rich models as observed in most GCs. For both normal and He-rich abundances we calculate models with a scaled solar composition and with a chemical composition typical of the second-population GC stars ([C/Fe] = [O/Fe] = −0.6, [N/Fe] =+1.0, [Na/Fe] =+1.0). This abundance pattern was made to reproduce observed GC abundances due to multiple populations (e.g. Carretta et al. 2009a) with the constraint that the C+N+O and Ne+Na abundances are kept constant (as observed in most GCs; e.g. Brown, Wallerstein & Oke 1991; Dickens et al. 1991; Norris & Da Costa 1995; Smith et al. 1996; Ivans et al. 1999; Cohen & Meléndez 2005; Yong, Grundahl & Norris 2015).

We follow Conroy & van Dokkum (2012a) and used the 2012 version of the Dotter et al. (2007) isochrones for the main sequence (MS) through to the tip of the red giant branch (RGB). For post-RGB evolution we used the Bertelli et al. (2008) isochrones matched in age, helium content, and metallicity to the Dotter et al. (2007) models. However, the models from the two data base do not predict the same initial mass at the tip of the RGB. To prevent a discontinuity in the initial masses of the combined isochrones, we subtract the difference (∼0.01 $M_{\odot}$) from the initial masses of Bertelli et al. (2008) isochrones to match the Dotter et al. (2007) isochrones (as done in Conroy & van Dokkum 2012a). Our choice of isochones was dictated by the need to vary He and to have the models extend to low stellar masses. For each isochrone we selected semi-uniformly ∼100 points in $\log(L)$-$\log(T_{\rm eff})$ space covering all stages of stellar evolution from the lowest mass MS star to the end of the AGB phase. We selected more points from evolutionary phases such as the main sequence turn-off (MSTO) where there are sharp variations in the $\log(L)$-$\log(T_{\rm eff})$ space. We refined our selection such that no point contributes more than 2 per cent to the integrated light assuming a Kroupa (2001) IMF. We used the same isochones for the N, Na enhanced, C, O depleted and solar He models (referred as CNONa models hereafter, see Table 1) as for the solar composition models since stellar evolution is not affected by abundance variations of C, N, O, and Na if the C+N+O abundance is kept constant at fixed metallicity (as shown in Salaris et al. 2006; Coelho, Percival & Salaris 2011; Sbordone et al. 2011).

### 3.1 Initial-final mass relations

We investigate in this section the initial-final mass relation for our He-normal and He-rich models (cf. isochrones in Fig. 2). As previously discussed, the inclusion of the other abundance variations (such as C, N, O, Na) in our case does not influence the stellar evolution and in turn does not affect the initial-final mass relation. Thus, in this section we only refer to the He-normal and He-rich populations, but the results are transposable to the He-normal and He-rich populations with CNONa variations (referred as He-rich CNONa models hereafter). From the isochrones available, we can only take as final mass for stars ending their life as white-dwarf (WD) the core mass at the start of the thermally pulsing asymptotic giant branch. In this case, the final mass is slightly underestimated (Chantereau, Charbonnel & Meynet 2017), but since we are interested in differential effects between two model populations treated self-consistently, this approximation have only a negligible effect on the results.

For an initial helium content of 0.4, Chantereau et al. (2017) predict an average increase of the final mass of low-mass stars at low metallicity by ∼10 per cent (with respect to the final mass of He-normal stars). This result is fully consistent with an independent study from Althaus et al. (2017) using different mass-loss prescriptions, even though final masses are very sensitive to these prescriptions (see Fig. 3). This increase is rather constant as a function of the metallicity. Thus, since there are no predictions of the final mass of low mass stars at $Z_{\odot}$ for $Y_{\rm ini}$= 0.4, we assume here an average increase of the final mass of He-rich stars of ∼10 per cent for $M_{\rm ini} < 2.0$ $M_{\odot}$. At $Z_{\odot}$, Karakas (2014) found that 2.0–4.5 $M_{\odot}$ He-rich stars have an average core mass at the first thermal pulse ∼20 per cent higher than their He-normal counterpart. We assume the same increase for the final mass for stars with $M_{\rm ini}$ between 2 and 5 $M_{\odot}$. We then use a linear fit derived by least square fitting of these final masses to determine an initial-final mass relationship for both populations with $M_{\rm ini}$ between 0.5 and 7.0 $M_{\odot}$ (Fig. 4).

More massive stars end their life as neutron stars (NS) or black holes (BH, $M_{\rm ini}$>7.7 and 20 $M_{\odot}$, respectively; Belczynski et al. 2010), however for $Y_{\rm ini}$= 0.4, there are no available initial-final mass relations. But since these stars contribute only to a minority of all the mass locked in the cluster's remnants, it is reasonable to assume a similar initial-final mass relation for He-rich and He-normal stars for $M_{\rm ini} > 7.7 M_{\odot}$. Note that if we assume that NSs formed through electron-capture supernovae have the same minimum mass for both populations, then the minimum initial mass needed to form these NSs from He-rich progenitors is dramatically shifted down to ∼6.1$M_{\odot}$ (since the final mass of He-rich stars is greater than its He-normal counterparts for a given initial mass). Thus, the He enhancement will increase the formation rate of NSs through electron-capture supernovae (assuming an identical IMF), as pointed out in Shingles et al. (2015).

### 3.2 Stellar spectra and model atmosphere

We computed stellar model atmospheres, using ATLAS12 (Kurucz 1970, 2005), and synthesized stellar spectra using SYNTHE (Kurucz & Furenlid 1979; Kurucz & Avrett 1981). Both of these codes assume one-dimensional, static, and plane parallel atmospheres in local thermodynamic equilibrium. We used the same versions of these codes as in Martocchia et al. (2017) and refer the reader there for further details of our stellar atmosphere calculations. We synthesized the spectra over the 2000–10 000 Å wavelength range at a resolution of $R = 200\,000$ before using a Gaussian kernel to smooth it to $R = 5000$ for future analysis.

We calculated the spectral energy distribution for each chemical composition by splitting the mass range between 0.08 $M_{\odot}$ and the initial stellar mass of the AGB-tip (see e.g. Wachter et al. 2002; Kamath, Karakas & Wood 2012 for the terminology; 0.967 and 0.735 $M_{\odot}$ for the $Y_{\rm ini} = 0.26$ and the $Y_{\rm ini} = 0.4$ models, respectively) into bins centred on each of the stellar spectral models. We then summed together the model stellar spectral energy distributions weighted by the initial stellar mass in each bin according to a Kroupa (2001) IMF to produce the model spectral energy distribution for the population. We also calculated bottom heavy (dwarf star rich) solar composition models using power-law IMFs with a slope of $\alpha = -3.0$, $\alpha = -2.7$, and $\alpha = -2.35$ (Salpeter 1955). To compare our models with non-scaled solar chemistry with the effects of age and metallicity, we also calculated a model with lower metallicity

Downloaded from https://academic.oup.com/mnras/article-abstract/478/2/2368/4995915
by Liverpool John Moores University user
on 10 July 2018

**Table 1.** Stellar population models.

| Name<br>(1) | Helium<br>(2) | CNONa<br>(3) | [Fe/H]<br>(4) | Age (Gyr)<br>(5) | IMF<br>(6) |
|---|---|---|---|---|---|
| He-normal/solar | $Y_{\rm ini} = 0.26$ | 0 per cent | 0.0 | 12.6 | Kroupa |
| He rich | $Y_{\rm ini} = 0.40$ | 0 per cent | 0.0 | 12.6 | Kroupa |
| He-rich CNONa | $Y_{\rm ini} = 0.40$ | 100 per cent | 0.0 | 12.6 | Kroupa |
| CNONa | $Y_{\rm ini} = 0.26$ | 100 per cent | 0.0 | 12.6 | Kroupa |
| Bottom heavy | $Y_{\rm ini} = 0.26$ | 0 per cent | 0.0 | 12.6 | $\alpha = -3.0$ |
| $\alpha = -2.7$ IMF | $Y_{\rm ini} = 0.26$ | 0 per cent | 0.0 | 12.6 | $\alpha = -2.7$ |
| Salpeter IMF | $Y_{\rm ini} = 0.26$ | 0 per cent | 0.0 | 12.6 | $\alpha = -2.35$ |
| Younger | $Y_{\rm ini} = 0.26$ | 0 per cent | 0.0 | 8.9 | Kroupa |
| Metal poor | $Y_{\rm ini} = 0.26$ | 0 per cent | −0.3 | 12.6 | Kroupa |
| He-rich CNONa 5 per cent | 95 per cent $Y_{\rm ini} = 0.26$ + 5 per cent $Y_{\rm ini} = 0.40$ | 5 per cent | 0.0 | 12.6 | Kroupa |
| He-rich CNONa 10 per cent | 90 per cent $Y_{\rm ini} = 0.26$ + 10 per cent $Y_{\rm ini} = 0.40$ | 10 per cent | 0.0 | 12.6 | Kroupa |
| He-rich CNONa 20 per cent | 80 per cent $Y_{\rm ini} = 0.26$ + 20 per cent $Y_{\rm ini} = 0.40$ | 20 per cent | 0.0 | 12.6 | Kroupa |
| He-rich CNONa 50 per cent | 50 per cent $Y_{\rm ini} = 0.26$ + 50 per cent $Y_{\rm ini} = 0.40$ | 50 per cent | 0.0 | 12.6 | Kroupa |
| ETG mix | 95 per cent $Y_{\rm ini} = 0.26$ + 5 per cent $Y_{\rm ini} = 0.40$ | 27.5 per cent | 0.0 | 12.6 | Kroupa |

*Notes*. Column (1): Model name. Column (2): Initial helium mass fraction. Column (3): Percentage of N, Na enhanced, and C, O depleted stars. Column (4): Metallicity. Column (5): Age in Gyr. Column (6) IMF. Kroupa means a (Kroupa 2001) IMF while $\alpha = -3.0$, $\alpha = -2.7$, and $\alpha = -2.35$ are power-law IMFs with the given slopes.

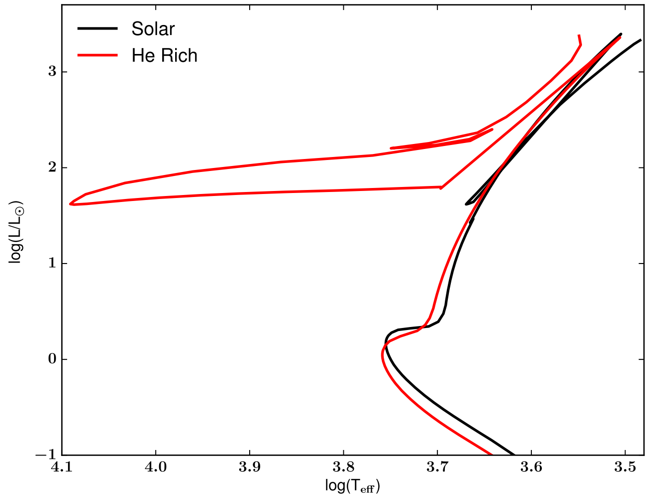

**Figure 2.** Isochrones at $Z_\odot$ and 12.6 Gyr for He-normal and He-rich populations (black and red, respectively). The He-rich isochrone has a significantly hotter horizontal branch as well as a slightly hotter main sequence, red giant branch, and asymptotic giant branch.

([Fe/H] = −0.30) as well as a model with a younger age (8.9 Gyr) at solar composition.

Here we have chosen for the second-population stars a $Y_{\rm ini}$ as high as 0.4, to cover the extreme value found in a few Galactic GCs (NGC 2808, $\omega$ Cen, NGC 6388, and to a certain extent NGC 2419; Busso et al. 2007; King et al. 2012; Di Criscienzo et al. 2015; Milone et al. 2015). However, ETGs likely possess a range of He abundances rather than the two extreme values we consider, thus we have also interpolated from these two values a mixture of He-normal models with 5, 10, 20, and 50 per cent of He-rich CNONa models. We also create a population more representative of the core of ETGs (see Section 2) made up of ∼35 per cent second-population stars by combining our models. We model the He-rich population by representing the 5 per cent fraction of stars with $\Delta Y > 0.1$ with our $Y$= 0.4 model (He-rich CNONa model). Of the remaining 30 per cent of second-population stars, we assume that half have extreme chemistry but solar He (CNONa model), and the other half have intermediate chemistry which we represent with a 50–50 mix of our solar model and the CNONa model. Thus, we approximate the expected chemistry of the centre of a massive ETG with a mixture that is 5 per cent He-rich CNONa, 22.5 per cent CNONa, and 72.5 per cent solar composition.

### 3.3 Magnitudes and spectral indices

To quantify large-scale differences between the spectral energy distribution of our different models, we calculated synthetic photometry by convolving each of the stellar population spectral energy distributions with the Hubble Space Telescope Wide Field Camera 3 (WFC3) filter curves[2]. We used the photometric zero-points provided by the instrument website[3] to calculate magnitudes in the Vega system (F225W, F275W, F336W, F438W, F475W, F555W, F606W, F625W, F775W, F814W, F850LP).

To study how a range of spectral features varies between models, we also calculated a range of Lick indices (Worthey et al. 1994) and indices used in IMF studies (e.g. Maraston et al. 2003; Conroy & van Dokkum 2012a). We calculated indices both sensitive to the IMF (e.g. Na D, Na 8190, and CaT) and insensitive (e.g. H$\beta$ and Fe 5270). Before calculating line strength indices, we broadened our model spectra to a velocity dispersion of 250 km s$^{-1}$. We then used the index definitions displayed in Table 2 and the formula provided in Cenarro et al. (2001) to calculate the index strengths. As we are interested only in the differences between models, we do not attempt to place our Lick indices on the Lick system.

### 3.4 Caveats to the modelling

In our stellar population synthesis models, we did not take into account variations of Mg and Al initial abundances. This is motivated by the fact that the Mg–Al anticorrelation is not an ubiquitous chemical feature in GCs (see e.g. Carretta et al. 2009b). In addition,

---

[2] http://www.stsci.edu/hst/wfc3/ins_performance/throughputs/Throughput_Tables

[3] http://www.stsci.edu/hst/wfc3/analysis/uvis_zpts

Downloaded from https://academic.oup.com/mnras/article-abstract/478/2/2368/4995915
by Liverpool John Moores University user
on 10 July 2018

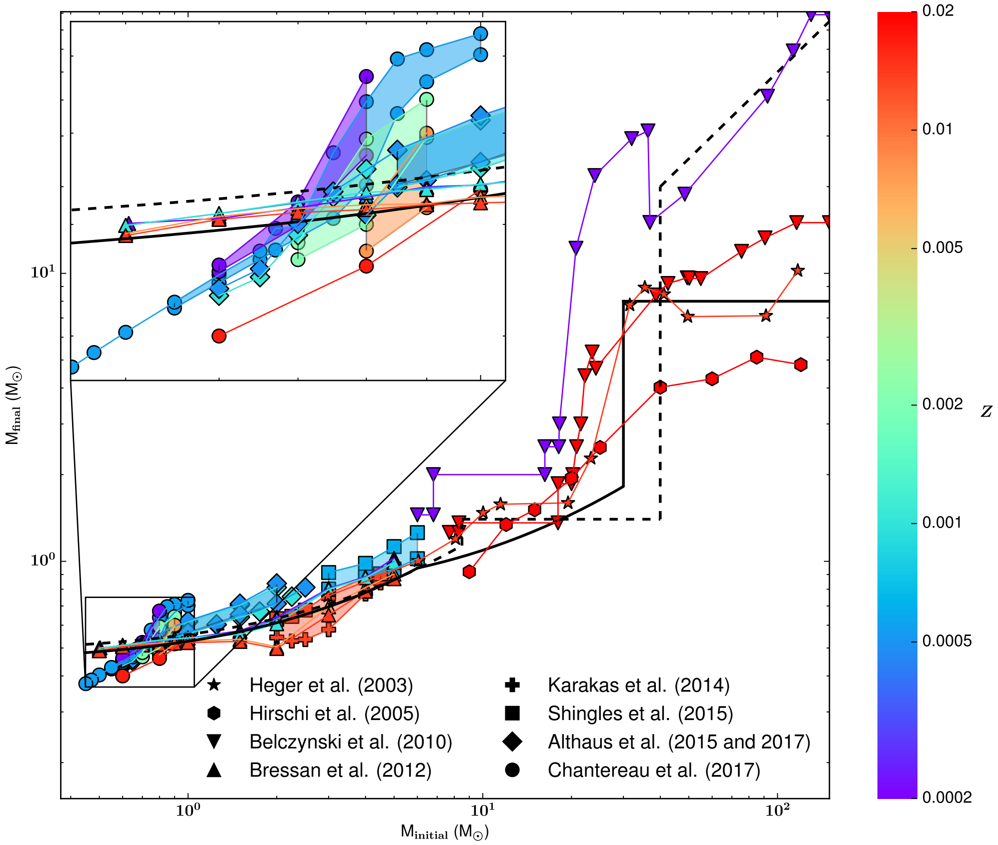

**Figure 3.** Theoretical predictions from the literature for initial-final mass relations at several metallicities (colour-coded). The relation from Renzini & Ciotti (1993) represented by a black dashed line is a standard prescription used in stellar population synthesis (e.g. Maraston 1998; Conroy et al. 2009). The GALEV evolutionary synthesis model (Kotulla et al. 2009) is represented by a continuous black line. The filled areas correspond to differences between He-normal and He-rich ($Y_{\rm ini} = 0.4$) predictions.

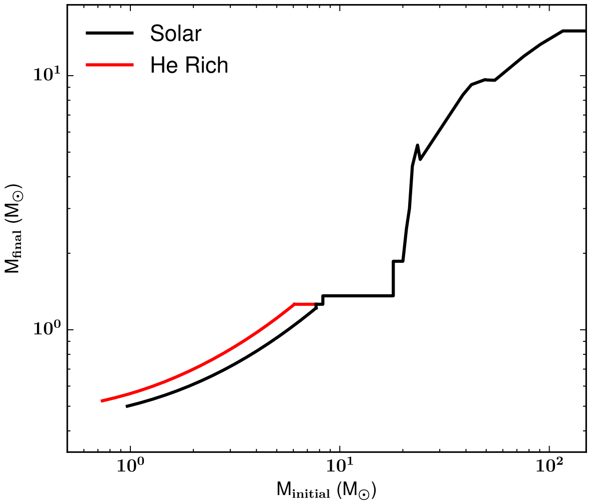

**Figure 4.** Initial-final mass relationship as a function of $M_{\rm ini}$ for He-normal and He-rich stars (black and red, respectively) at Z$_\odot$ and 12.6 Gyr.

Cassisi et al. (2013) showed that the inclusion of Mg and Al abundance variations in stellar models and synthetic spectra has only a small effect on bolometric corrections in standard filters. We also assume the same surface abundances at all stages of stellar evolution. Thus, we do not consider the effects of several processes, including diffusion, convective mixing, and radiative levitation, that modify the surface chemistry of a star as it evolves. But since we are interested here in differences between He-normal and He-rich models, it will not largely affect our results under the rough assumption that these processes have similar effects on both populations. However, this assumption may be violated for the horizontal branch stars in our He-rich models that are at the onset (∼12 000 K) of the effects of radiative levitation (e.g. Behr 2003; Pace et al. 2006). The simple models we present in this study do not account for blue stragglers, post-AGB stars, and binaries, but their effects are briefly discussed in Section 7.

Since we are mainly interested in the changes in the spectral energy distribution due to chemical composition, we are less sensitive to the limitations of calculating synthetic spectra (incomplete line lists, etc.) that are especially important for cool stars. We only model stellar photospheres; however, chromospheres can play an important role for some spectral features and the ultraviolet luminosity in cool stars (Wedemeyer et al. 2017). While the effects of non-local thermal equilibrium can be significant for some spectra features (e.g. Asplund 2005; Short, Young & Layden 2015), the effects of non-local thermal equilibrium on the response to abundance changes are not significant (Conroy et al. 2018). In addition, the solar abundance patterns adopted by the isochrones are slightly different from the ones we use for our stellar atmosphere calculations. Finally, we would like to note that stellar atmosphere modelling of cool stars is less accurate than for stars with higher temperature, which is a recurrent problem in stellar population synthesis studies. However, since here we are interested in differences between two

Downloaded from https://academic.oup.com/mnras/article-abstract/478/2/2368/4995915
by Liverpool John Moores University user
on 10 July 2018

**Table 2.** Spectroscopic Index definitions.

| Index<br>(1) | Feature [Å]<br>(2) | Continuum [Å]<br>(3) | Notes<br>(4) |
|---|---|---|---|
| Ca HK | 3898.4–4002.4 | 3805.4–3832.7<br>4019.6–4051.3 | S05 |
| H$\delta$ | 4083.5–4122.3 | 4041.6–4079.8<br>4128.5–4161.0 | Lick |
| $CN_1$ | 4142.1–4177.1 | 4080.1–4117.6<br>4244.1–4284.1 | Lick |
| CH 4300 | 4281.4–4316.4 | 4266.4–4282.6<br>4318.9–4335.1 | Lick |
| Fe 4383 | 4369.1–4420.4 | 4359.1–4370.4<br>4442.9–4455.4 | Lick |
| H$\beta$ | 4847.9–4876.6 | 4827.9–4847.9<br>4876.6–4891.6 | Lick |
| $Mg_1$ | 5069.1–5134.1 | 4895.1–4957.6<br>5301.1–5366.1 | Lick |
| $Mg_b$ | 5160.1–5192.6 | 5142.6–5161.4<br>5191.4–5206.4 | Lick |
| Fe 5270 | 5245.7–5285.7 | 5233.2–5248.2<br>5285.7–5318.2 | Lick |
| Na D | 5876.9–5909.4 | 5860.6–5875.6<br>5922.1–5948.1 | Lick |
| $TiO_1$ | 5936.6–5994.1 | 5816.6–5849.1<br>6038.6–6103.6 | Lick |
| Na 8190 | 8174.7–8202.7 | 8167.7–8174.7<br>8202.7–8212.7 | C12 |
| CaT | 8484.0–8513.0<br>8522.0–8562.0<br>8642.0–8682.0 | 8474.0–8484.0<br>8563.0–8577.0<br>8619.0–8642.0<br>8700.0–8725.0<br>8776.0–8792.0 | C01 |
| PaT | 8461.0–8474.0<br>8577.0–8619.0<br>8730.0–8772.0 | 8474.0–8484.0<br>8563.0–8577.0<br>8619.0–8642.0<br>8700.0–8725.0<br>8776.0–8792.0 | C01 |
| TiO 8860 | | 8832.6–8852.6<br>8867.6–8887.6 | C12 |

*Notes:* Column (1): Index name. Column (2): Feature passband(s). Column (3): Continuum passbands. Column (4): C01: Cenarro et al. (2001), C12: Conroy & van Dokkum (2012a), Lick: Lick index (Worthey et al. 1994; Worthey & Ottaviani 1997) S05: Serven, Worthey & Briley (2005). The TiO 8860 index was defined by Conroy & van Dokkum (2012a) as the ratio of fluxes between blue and red passbands.

populations with different initial chemical compositions, the effects on the results are mitigated.

## 4 MASS-TO-LIGHT RATIO

First, we determine the stellar mass for populations with different chemical compositions, initial mass functions, and ages. We assume that gas lost during stellar evolution – stellar winds and supernovae ejecta – is expelled from the stellar population. At $Z_\odot$, 12.6 Gyr, and for a normal initial helium content, all the stars with $M_{\rm ini} \geq 0.967\ M_\odot$ are present in the form of remnants whereas for a higher initial helium content of 0.4 this transition is shifted down to $M_{\rm ini} = 0.735\ M_\odot$. This is due to the well-known fact that He-rich stars have shorter lifetimes than their He-normal counterparts (e.g. Salaris et al. 2006; Pietrinferni et al. 2009; Sbordone et al. 2011; Valcarce, Catelan & Sweigart 2012; Chantereau, Charbonnel & Decressin 2015; Althaus et al. 2017). The total mass locked in remnants from He-rich progenitors is then higher by ∼41 per cent with respect to the He-normal population (+0.062 $M_\odot$ when the initial mass of the population is normalized to 1 $M_\odot$). The inclusion of the mass-loss during advanced phases does not significantly change the total mass of stars since there are only 3 per cent and 3.5 per cent of post-MS stars (in mass) for $Y_{\rm ini}= 0.26$ and 0.4, respectively. Thus, the fact that the mass-loss dependence on the initial helium content is currently unknown does not affect our conclusions for the total stellar mass. The total mass of stars still in the nuclear burning phase of the He-rich population is then lower by ∼14 per cent with respect to the He-normal population (−0.055 $M_\odot$ when normalized to 1 $M_\odot$), which counterbalanced the mass locked into remnants. We can then conclude that at 12.6 Gyr and at $Z_\odot$, the mass of both He-normal and He-rich populations are very similar.

For a younger He-normal population (8.9 Gyr), only stars with $M_{\rm ini} \leq 1.035\ M_\odot$ are still in the nuclear burning phase, which is relatively close to our old He-normal population. Thus, an age difference of 3.7 Gyr has only a negligible effect on the total mass of the population. At a lower metallicity of [Fe/H] = −0.3, He-normal stars that are still in the nuclear burning phase have a maximum initial mass very similar to the He-normal case at $Z_\odot$. As shown in Fig. 3, since the initial-final mass relation does not change between $Z_\odot$ and [Fe/H] = −0.3 ($Z = 0.0069$), we keep the same relation used before. Therefore, the total mass of the He-normal population is the same as in the solar metallicity case. Finally we also compute the mass for a range of bottom heavy IMFs ($\alpha = -3.0$, −2.7, and −2.35) at $Z_\odot$ and 12.6 Gyr. As the slope of the IMF steepens, a higher fraction of the initial stellar mass is still in nuclear active stars. Thus, the normalized mass (to 1 $M_\odot$) of the population approaches unity.

Our model spectral energy distributions are displayed in Fig. 5. The shape of the solar composition bottom heavy IMF model ($\alpha = -3$) is almost identical to the solar composition Milky Way-like IMF one (Kroupa 2001) but the bottom heavy model is much fainter for the same initial mass. The He-rich model is dramatically brighter than the He-normal model bluewards of 2600 Å, brighter at wavelengths bluer than ∼5000 Å, but fainter redwards. The CNONa models have similar-shaped spectral energy distributions to solar models (same He abundance) but differ in the strengths of several spectral features, including molecular bands and strong Na lines. Finally both the metal poor and the younger models are brighter and bluer than our old, solar metallicity model but not as bright as the He-rich models in the ultraviolet.

Colour–colour plots for our models are displayed in Fig. 6. Changing from a Milky Way-like IMF to a bottom heavy IMF has little effect on the colours except (F606W−F814W), which is slightly redder. As expected from the spectral energy distributions, enhanced He models have bluer colours compare to models with solar metallicities. Younger ages and lower metallicities also lead to bluer colours, but not as blue as the He-rich models. CNONa abundances lead to slightly bluer colours except in (F336W−F438W), which is marginally redder than the solar composition model.

The mass-to-light ratios for our different models are displayed in Table 3 and Figs 7 and 8. Since we have shown that He, CNONa, age (up to a 3.7 Gyr spread), and metallicity (up to Δ[Fe/H] = −0.3) do not dramatically affect the total stellar mass, *M*/*L* mainly depends on differences in the light contribution. The He-rich population has a negligible effect on the *M*/*L* between *V* (F606W) and *I* (F814W) bands, which does not explain the variations found in the *r* band by Cappellari et al. (2012). We also find that the differences in *M*/*L* between the case where only $Y_{\rm ini}$ changes (He-rich model) with the case where all the initial abundances vary (He-rich CNONa model)

Downloaded from https://academic.oup.com/mnras/article-abstract/478/2/2368/4995915
by Liverpool John Moores University user
on 10 July 2018

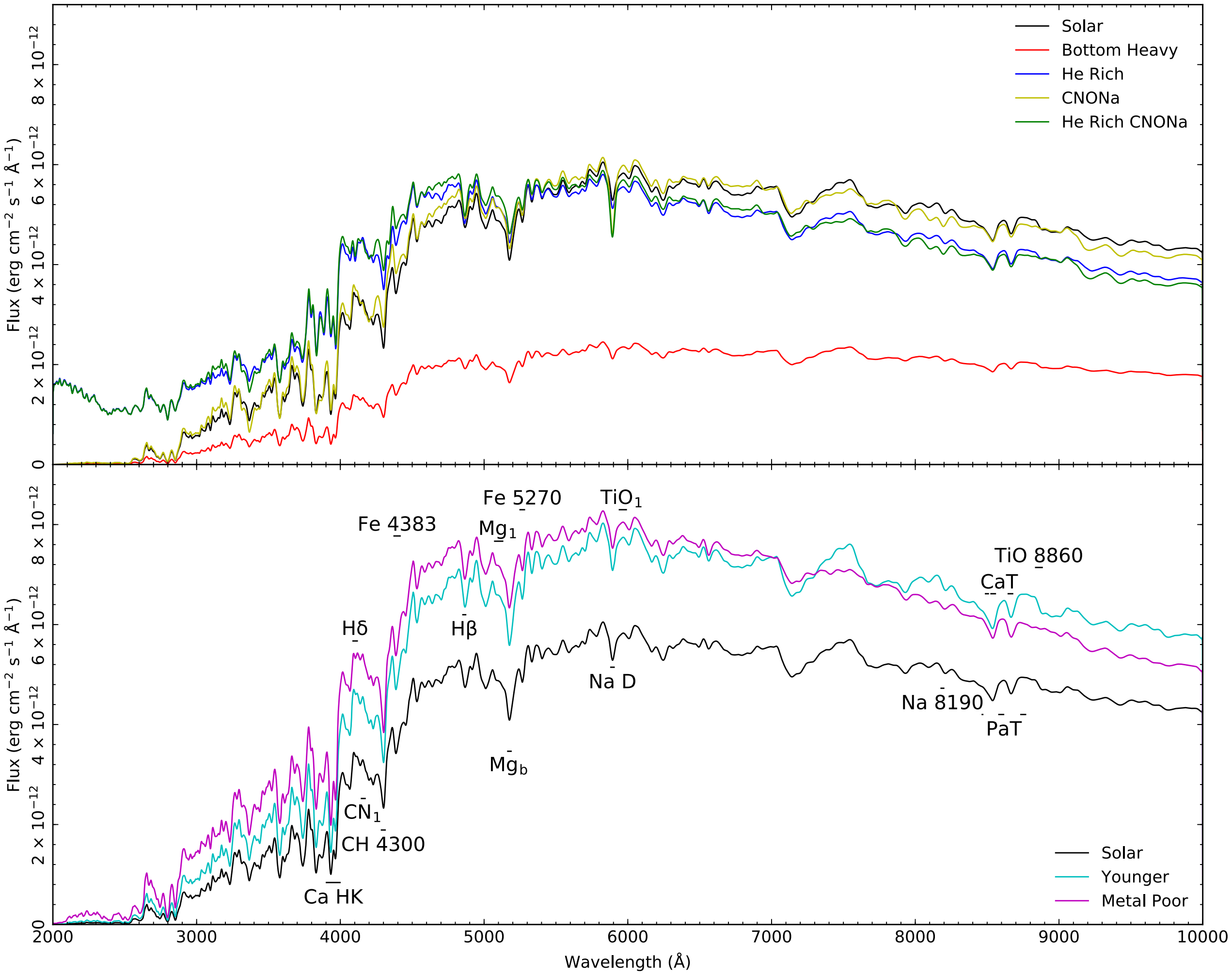

**Figure 5.** Model spectral energy distributions. *Top panel:* Effects of He, CNONa, and the IMF. The solar composition, Kroupa IMF, model is shown as a black line, the solar composition, bottom heavy IMF ($\alpha = -3.0$) model as a red line, the He-rich ($Y_{\rm ini}$= 0.4) model as a blue line, the enhanced NNa, depleted CO model as a yellow line and the HeNNa enhanced, depleted CO model as a green line. The bottom heavy IMF model is significantly fainter than the Kroupa IMF model but has a similar-shaped spectral energy distribution. The He-rich models are bluer than the He-normal models, especially shortwards of 3000 Å. The CNONa models are broadly similar to the models with the same He abundances but differ in the strengths of Na and molecular features. *Bottom panel:* Effects of age and metallicity. The solar metallicity, 12.6 Gyr model is shown as a black line, the younger 8.9 Gyr model as a cyan line, and the subsolar metallicity ([Fe/H] = −0.3) model as a magenta line. Both the metal-poor and the younger models are brighter and bluer than the reference model and have weaker metal lines and molecular bands as well as stronger Balmer lines. Each spectrum has been smoothed to a spectral resolution of $R = 200$ for the purposes of display and represents the flux from 1 M$_\odot$ of initial stellar mass.

are negligible, highlighting the fact that as expected He is the main factor of *M*/*L* variations in the different filters. As expected (e.g. Conroy, Gunn & White 2009), more bottom heavy IMFs lead to higher *M*/*L* in all bands. The ratio of the *M*/*L* of a model with a bottom heavy IMF to a population with the same chemistry and a Milky Way-like IMF is largely insensitive of wavelength. Therefore, here we can safely rule out the He-rich population as the source of the *M*/*L* variations in *r* band (F625W) in massive ETGs.

Both the younger and more metal-poor models display similar behaviour to the He-rich population in that their *M*/*L* decreases with shorter wavelengths. However, unlike an He-rich population, the younger and metal poor models show lower *M*/*L* with respect to the old, solar metallicity model in the *V* band (F606W) and redwards. The 5, 10, and 20 per cent models are close to the He-normal case in most of the bands. However, a conservative mixture such as 95 per cent of He-normal stars with 5 per cent of He-rich stars still leads to relatively large differences of *M*/*L* in the ultraviolet bands. The He-rich population leads to a near-UV luminosity (in the F225W filter) ~20 times higher than for the He-normal population and ~2 times higher if we take only 5 per cent of He-rich stars into account. This is in good agreement with the statement that He-rich populations in ETGs could play an important role in the UV-excess phenomenon (e.g. Code & Welch 1979; Burstein et al. 1988; Greggio & Renzini 1990; Dorman et al. 1995; Brown et al. 1997; O'Connell 1999; Brown et al. 2000).

## 5 SPECTRAL INDICES

We plot the spectral index measurements for our models in Figs 9 and 10. We note that the strength of a spectral index depends not just on the spectral feature that dominates the index, but on all atomic and molecular lines present in both the feature and continuum passbands. While spectral indices fail to capture all information available in the spectral energy distribution – they ignore the shape of

Downloaded from https://academic.oup.com/mnras/article-abstract/478/2/2368/4995915
by Liverpool John Moores University user
on 10 July 2018

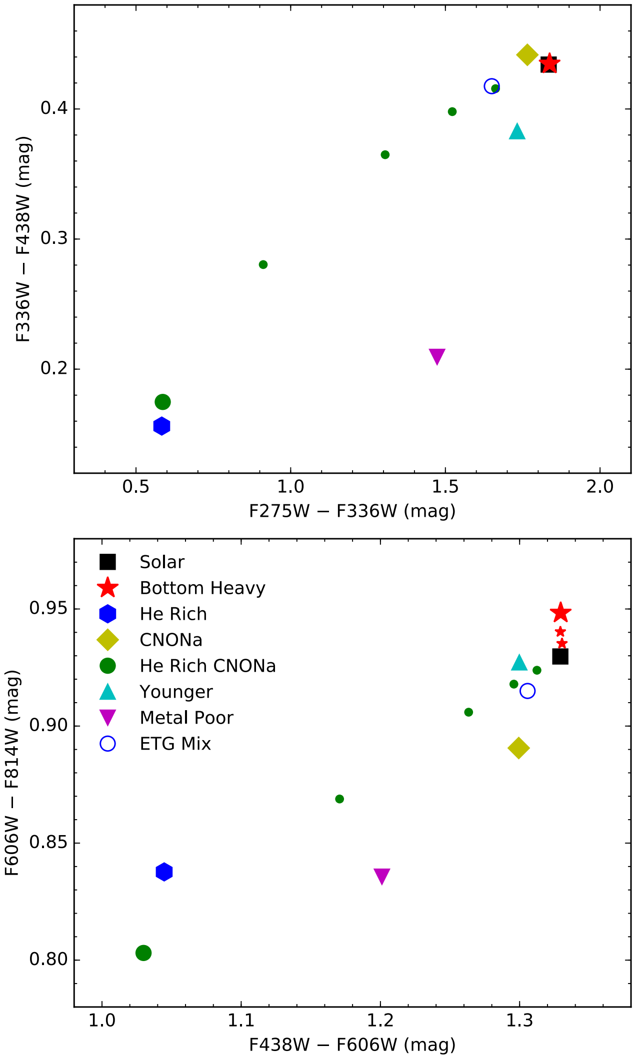

**Figure 6.** Colour–colour plots for our models in the HST WFC3 passbands. The solid black square is the solar composition model, the red star is the bottom heavy IMF model ($\alpha = -3.0$), the blue hexagon is the He-rich model, the yellow diamond is the CNONa abundance pattern model ([C/Fe] = [O/Fe] = −0.6, [N/Fe] =+1.0, [Ne/Fe] = −0.07, [Na/Fe] =+1.0), the green circle is the He-rich CNONa pattern, the cyan upwards triangle is the younger model (8.9 Gyr), and the magenta downwards pointing triangle is the metal-poor model ([Fe/H] = −0.3). The small green circles represent mixtures of the solar composition model with 5, 10, 2, or 50 per cent of the He-rich CNONa abundance pattern. The small red stars between the solar composition, Kroupa IMF model, and the bottom heavy IMF model are the Salpeter ($\alpha = -2.35$) and $\alpha = -2.7$ IMF models, respectively. The hollow blue circle represents our ETG mixture model (22.5 per cent CNONa model, 5 per cent He-rich CNONa model, 72.5 per cent solar model). He-rich models are bluer than solar He models across all colours as are the younger model and the metal-poor model. The bottom heavy IMF model has similar colours to the Milky Way-like IMF solar composition model except in (F606W−F814W) where it is slightly redder. The CNONa model shows slightly bluer colours with respect to the solar composition model except in (F336W−F438W) where the CNONa model is slightly redder. We note that the F336W, F438W, F606W and F814W WFC3 filters approximate the *UBVI* Johnson–Cousins filters.

the spectral feature being measured – they do provide insights into the effects of varying various stellar population parameters (Conroy & van Dokkum 2012a).

Our models confirm the previous work on the effects of age, metallicity, and the IMF on spectral indices. In line with previous work (e.g. Worthey 1994; Bruzual & Charlot 2003; Thomas, Maraston & Bender 2003; Schiavon 2007), young populations, and more metal-poor populations generally have weaker metal lines and stronger hydrogen Balmer lines with age having a stronger effect on the hydrogen lines and metallicity having a stronger effect on the metal lines and molecular bands. The effects of a bottom heavy IMF on our modelled spectral indices are also broadly consistent with the previous work (e.g. Conroy & van Dokkum 2012a; La Barbera et al. 2013) with spectra features strong at low surface gravities, such as the CaT, are weaker in the bottom heavy models and spectral features stronger at high surface gravities, such as the Na doublets at 5890 and 8190 Å, are stronger. As has been previously shown, the IMF generally has little effect on spectral features in the blue portion of the optical wavelength range although some molecular bands such as the MgH band at 5100 Å (which affects both the $\mathrm{Mg}_1$ and $\mathrm{Mg}_b$ indices) do show an IMF dependence.

The effect of He enhancement on Lick indices has also been considered in the previous work (e.g. Schiavon et al. 2004; Chung et al. 2013; Chung, Yoon & Lee 2017). As in previous studies we see significantly stronger Balmer lines in the He-rich models. Enhanced He also leads to weaker metal lines, particularly at shorter wavelengths. An exception to this trend is the CaT where the presence of the Pa 13, Pa 15, and Pa 16 hydrogen Paschen lines overlaps in wavelength with the three CaT lines. The enhanced He abundance leads to stronger Paschen absorption that causes a stronger CaT index strength although the strength of the CaT lines themselves is barely affected by the He enhancement.

These changes in line strength with He are mostly due to the effects of He on the horizontal branch as the main sequence and giant branches of the He-rich model are only ∼200 K hotter than the solar composition model while the horizontal branch of the He-rich model is 7600 K hotter than the red clump of the solar He model (12300 K versus 4700 K). We note that the morphology of the horizontal branch is dependent on a host of factors besides He abundance including age and metallicity as well as the amount of mass loss on the RGB. Thus, the effect of enhanced He varies with age and metallicity (e.g. Chung et al. 2017). We note that a population with a hotter horizontal branch would likely have weaker H lines than our He-rich model due to the increased ionization of H with increasing temperature. While to first order the effects of increased He mimic the effects of younger ages, more detailed comparisons do revel differences (Schiavon et al. 2004; Schiavon 2007).

Unsurprisingly, the Na D and Na 8190 indices are significantly stronger in CNONa models. Since N is the minority species, the $\mathrm{CN}_1$ index is significantly stronger in the CNONa models while the C-dominated CH 4300 index is weaker. Although the strength of TiO bands is mainly set by the Ti abundance, the lower O abundance in the CNONa models leads to weaker $\mathrm{TiO}_1$ and TiO 8860 bands. We note the conversion of Ne into Na in the CNONa models has an important second-order effect on many spectral features by raising the electron pressure as Na has a relatively low (5.1 eV) ionization potential while Ne has a relatively high (21.6 eV) ionization potential (Conroy & van Dokkum 2012a). Changes in the abundances of the CNO elements also play a secondary role in affecting index strengths by changing the strengths of molecular bands in both the feature passbands and the continuum passbands. An example

Downloaded from https://academic.oup.com/mnras/article-abstract/478/2/2368/4995915
by Liverpool John Moores University user
on 10 July 2018

**Table 3.** Mass locked in the remnants and the stars (normalized to 1 $M_\odot$) and *M*/*L* in different WFC3 filters while the closest filters in the SDSS and Johnson-Cousins systems are displayed in brackets.

| Models | Mass | F225W | F336W (U/u) | F438W (B) | F475W (g) | F555W (V) | F625W (r) | F775W (i) | F814W (I) | F850LP (z) |
|---|---|---|---|---|---|---|---|---|---|---|
| Solar | 0.568 | 17.73 | 9.88 | 6.50 | 5.36 | 4.67 | 3.98 | 3.07 | 2.89 | 2.45 |
| He rich | 0.560 | 0.86 | 6.02 | 5.12 | 4.80 | 4.54 | 4.17 | 3.39 | 3.22 | 2.78 |
| He rich CNONa | 0.560 | 0.86 | 5.93 | 4.96 | 4.66 | 4.45 | 4.12 | 3.43 | 3.27 | 2.85 |
| CNONa | 0.568 | 16.12 | 9.48 | 6.20 | 5.16 | 4.55 | 3.92 | 3.11 | 2.94 | 2.51 |
| Bottom Heavy | 0.944 | 72.93 | 40.56 | 26.68 | 22.06 | 19.19 | 16.32 | 12.43 | 11.67 | 9.82 |
| Younger | 0.575 | 10.48 | 6.98 | 4.81 | 4.02 | 3.53 | 3.04 | 2.35 | 2.21 | 1.86 |
| Metal Poor | 0.568 | 4.59 | 5.13 | 4.15 | 3.62 | 3.27 | 2.90 | 2.37 | 2.27 | 2.00 |
| He-rich CNONa 5 per cent | 0.567 | 9.01 | 9.56 | 6.40 | 5.32 | 4.66 | 3.99 | 3.09 | 2.91 | 2.47 |
| He-rich CNONa 10 per cent | 0.567 | 6.03 | 9.27 | 6.31 | 5.28 | 4.65 | 3.99 | 3.11 | 2.93 | 2.49 |
| He-rich CNONa 20 per cent | 0.566 | 3.63 | 8.73 | 6.12 | 5.21 | 4.62 | 4.01 | 3.14 | 2.96 | 2.52 |
| He-rich CNONa 50 per cent | 0.564 | 1.65 | 7.43 | 5.63 | 4.99 | 4.56 | 4.05 | 3.24 | 3.07 | 2.63 |

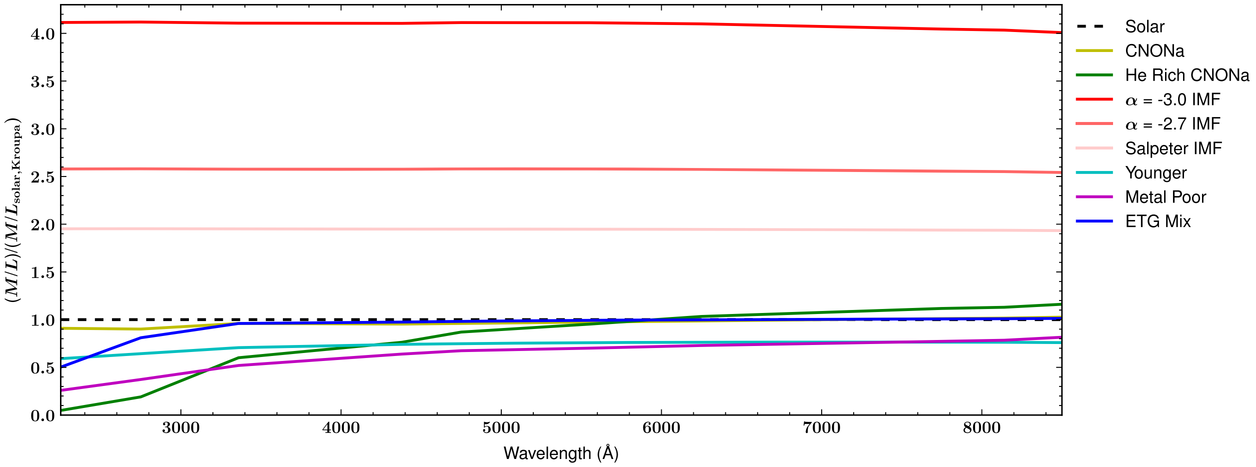

**Figure 7.** Mass-to-light ratio as a function of wavelength. *M*/*L* for the solar composition, Milky Way-like IMF model (black), the bottom heavy IMF model (red), the CNONa model (yellow); the He-rich CNONa model (green), the younger (8.9 Gyr) model (cyan), the metal poor ($[\mathrm{Fe/H}] = -0.3$) model (magenta), and finally the ETG mixture model (blue). The He-rich solar model (not displayed here) is largely similar to the He-rich CNONa model. The bottom heavy IMF ($\alpha = -3.0$) has a higher *M*/*L* with respect to the Milky Way IMF model with a similar ratio ($\sim$4) between the two models at all wavelengths. The He-rich CNONa model has a significantly lower *M*/*L* at the bluest wavelengths than the solar model but slightly higher *M*/*L* at the reddest wavelengths. Increasing N and Na, while decreasing C and O, has little effect on the *M*/*L* at either solar or high He. Both the younger and metal-poor models show lower *M*/*L* with respect to the old, solar metallicity model at all wavelengths but show relatively lower *M*/*L* values in the bluer bands.

of both these effects is the impact of NNa enhancement and CO depletion on the CaT index. The higher electron pressure caused by the enhanced Na abundance lowers the abundance of singly ionized Ca. This lowers the strength of the CaT lines themselves, while the lower O reduces the strength of the TiO bands in the region of the CaT and the increased N increases the strengths of the CN bands in the same region. Combined, these effects reduce the measured CaT strength.

To first order, the behaviour of the He-rich CNONa model is the superposition of the separate effects of He and of NNa enhancement with CO depletion. The models that are mixtures of the He-rich CNONa model and the solar composition model are intermediate to the two base models in rough proportion to the fraction of each model.

In the top panel of Fig. 11 we show both the hydrogen H$\beta$ index and the iron Fe 5270 for our models, which together have been commonly used to measure galaxy ages. Going from the solar composition, Kroupa IMF to a bottom heavy IMF model with the same chemistry has little effect on these indices. However, going from a solar composition model to the He-rich model leads to a large increase in H$\beta$ and a decrease in Fe 5270 in a similar manner to a younger age. The He-rich CNONa model shows the same behaviour.

In the bottom panel of Fig. 11 we show both the IMF-sensitive Na 8190 and CaT indices. While a bottom heavy IMF causes stronger Na 8190 and weaker CaT strengths, an increase in He leads to a stronger CaT index but almost no change in the Na 8190 index. However, the He-rich CNONa models show much stronger Na 8190

Downloaded from https://academic.oup.com/mnras/article-abstract/478/2/2368/4995915
by Liverpool John Moores University user
on 10 July 2018

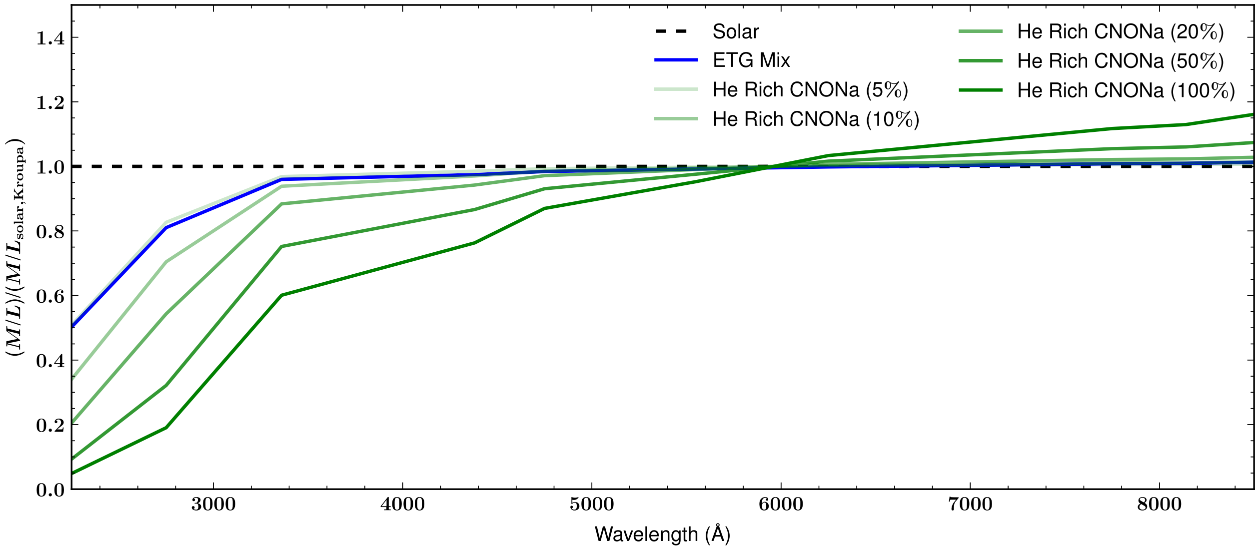

**Figure 8.** Mass-to-light ratio as a function of wavelength. The *M*/*L* for the solar composition model is plotted in black, for the He-rich CNONa model in green, and for the various mixtures of the He-rich CNONa model and the solar model as lighter shades of green. Unsurprisingly, the mixture models are intermediate to the two base models. The *M*/*L* for the ETG mixture model is plotted in blue.

indices and little change in the CaT strength. In Fig. 10, both the Mg indices and the TiO indices are stronger in the bottom heavy IMF models but weaker in the He-rich or CNONa models. Taken together, these plots show that increased He cannot explain the spectral feature evidence for a bottom heavy IMF. An He-rich population instead mimics the spectrum of a younger population. While an enhanced NNa and depleted CO population can mimic some of the effects of a bottom heavy IMF (i.e. enhanced Na indices), it cannot reproduce other indices (Mg indices, TiO bands).

## 6 EARLY-TYPE GALAXY MIXTURE

Unsurprisingly, the ETG mixture behaves similarly to the He-rich models and the CNONa models. While the shape of the spectral energy distribution of ETG mixture model is similar to CNONa model redwards ∼4000 Å, bluewards of ∼4000 Å the shape of the spectral energy distribution is similar to the He-rich CNONa model. This is most noticeable bluewards of 2500 Å where the flux of the ETG mixture model is over 3 times higher than the solar composition model. The *M*/*L* of the ETG mixture model is similar to the 5 per cent He-rich CNONa model as are the colours of the ETG mixture model. The increased He in our ETG mixture model leads to slightly stronger H indices in agreement with the other He-rich models (Fig. 9). Like the CNONa model, the CH, Mg, Ca, TiO, and Fe indices are weaker than the solar model while the CN and Na indices are stronger. In the H$\beta$–Fe 5270 plane (Fig. 11), the ETG mixture model follows the trend of the younger model rather than the bottom heavy IMF model. Thus ETG mixture model appears similar to the He-rich models in this plane.

However, in the Na 8190-CaT plane (Fig. 11), the ETG mixture behaves similar to the CNONa model and mimics the appearance of the bottom heavy IMF model. While observations solely of the Na 8190 doublet and the CaT of the ETG mixture model would suggest a bottom heavy IMF, observations that cover a wider range of spectral features such as the Mg indices and the TiO bands would not support such an interpretation. Thus, to disentangle chemical effects from IMF effects, we encourage the use of stellar population synthesis models such as Conroy & van Dokkum (2012a) that allow for the abundances of a wide range of elements to be varied and for observations that cover a wide wavelength range.

In our toy model, the CO depleted, NNa enhanced stars change the mass weighted mean abundances of the population from solar to [C/Fe] = [O/Fe] = −0.17 and [N/Fe] = [Na/Fe] =+0.28. These changes are comparable to the abundance differences between the centre and one effective radius observed in massive ETGs by van Dokkum et al. (2017), suggesting that disrupted GCs can play an important role in determining the mean abundances of the central regions of ETGs.

Disrupted GCs could also play a role in the origin of the UV-upturn. Several authors (e.g. Dorman, O'Connell & Rood 1995; Yi, Demarque & Oemler 1997; Peng & Nagai 2009) have proposed He-rich stars as the origin of the UV-upturn and GCs provide a source of such He-enhanced stars. The 5 per cent of He enhanced stars in our ETG toy model is sufficient to raise the near-UV F225W luminosity by a factor of 2. Hotter horizontal branch stars than those in our models (∼12 000 K), for example from lower metallicity but still highly He-enriched populations, produce even brighter far-UV and near-UV luminosities. We note that massive ETGs show broad GC metallicity distributions (e.g. Peng et al. 2006; Usher et al. 2012) and that such galaxies contain GCs with bright UV luminosities (e.g. Sohn et al. 2006; Rey et al. 2009; Bellini et al. 2015). Thus, disrupted GCs provide a plausible source for the UV bright stars responsible for the UV-upturn.

## 7 DISCUSSION

In this section, we briefly discuss the assumptions of our models and the perspectives. We have assumed that ETGs are single age and single metallicity. For a fixed mean age, extended star formation histories lead to bluer colours as younger populations are both bluer and brighter than older populations. While ETGs do display a spread in ages, studies of their star formation histories show that the most massive ETGs have at least 90 per cent of their mass in place by 10 Gyr ago (redshift of $z\sim 2$; e.g. Heavens et al. 2004; Panter et al. 2007; McDermid et al. 2015). The broad metallicity distribution present in ETGs (e.g. Harris & Harris 2002; Bird et al. 2010) leads

Downloaded from https://academic.oup.com/mnras/article-abstract/478/2/2368/4995915
by Liverpool John Moores University user
on 10 July 2018

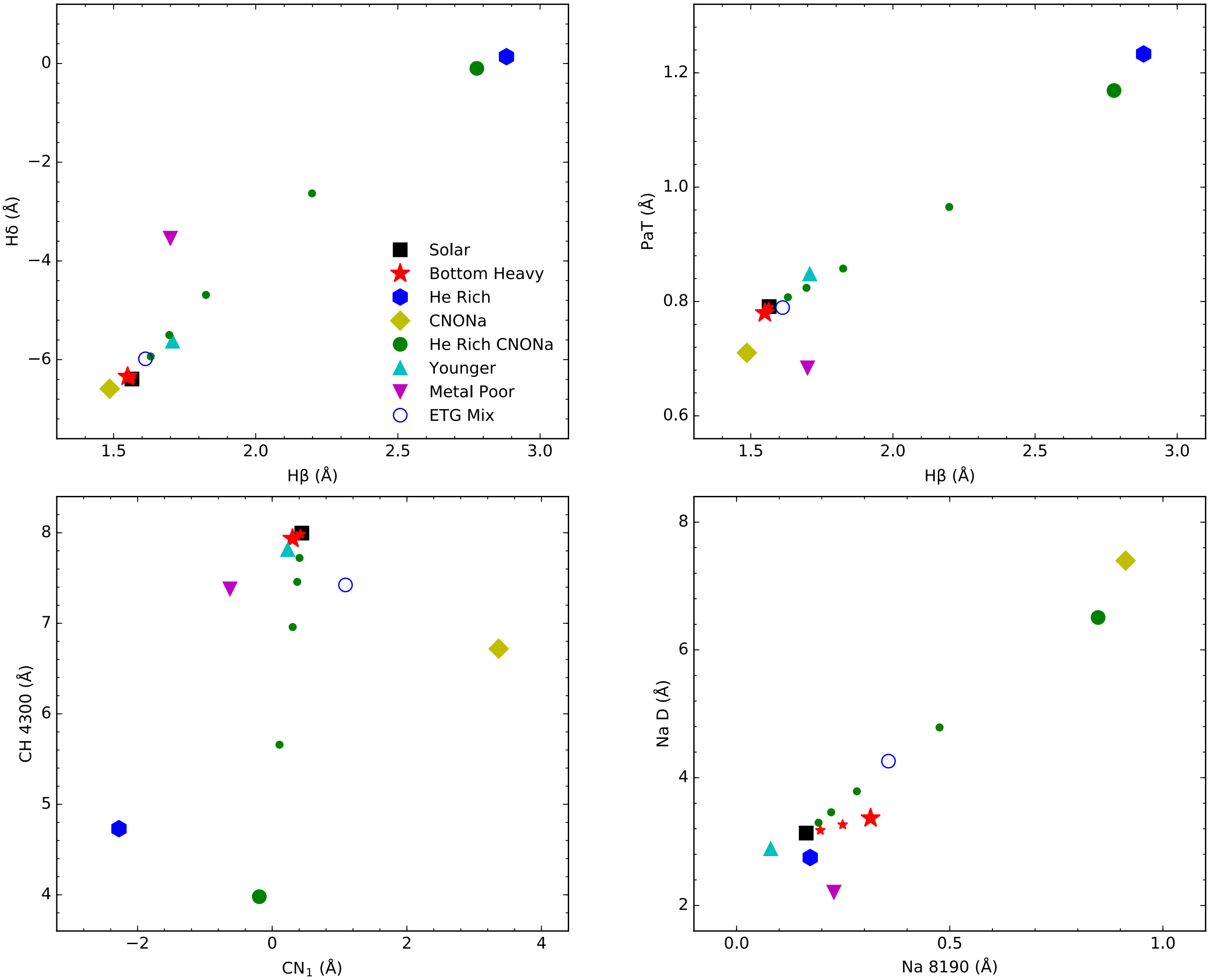

**Figure 9.** Line index strengths. The symbol shapes and colours are as in Fig. 6. *Top left:* Strength of the H$\delta$ line index versus the strength of the H$\beta$ line index. *Top right:* Strength of PaT Paschen line index versus the strength of the H$\beta$ line index. While the IMF has practically no effect on the strength of these H absorption lines, He abundance has a dramatic effect with an He-rich population mimicking a significantly younger population. The CNONa model displays slightly weaker H lines with respect to the solar composition model. *Bottom left:* Strength of the CH 4300 molecular index versus the strength of the CN$_1$ molecular index. While the IMF has virtually no effect on the strengths of the molecular bands, an He-rich population has weaker CH and CN bands. The C-poor and N-rich second population abundance pattern models unsurprisingly display weaker CH bands and stronger CN bands. *Bottom right:* Effects of He abundance on the Na D and Na 8190 line indices. While a bottom heavy IMF leads to stronger Na D and and Na 8190 absorption, enhanced He leads to weaker Na D lines but slightly stronger Na 8190 absorption. However, the effects of the IMF or He abundance on these Na indices are swamped by the effects of higher Na abundances in the second-population abundance pattern models.

to bluer colours in the ultraviolet than a narrow distribution with the same peak metallicity as lower metallicity populations are both brighter and bluer (Conroy, Gunn & White 2009; Tang, Worthey & Davis 2014).

The isochrones we use are not fully self-consistent since we use different data base for different stages of stellar evolution. This is due to the lack of stellar evolution models with enhanced helium that both extend to low stellar masses ($\sim$0.1 M$_{\odot}$) and fully cover post-RGB evolution.

The models we present in this study do not account for blue stragglers (BSs), post-AGB stars, and binaries. BSs dominate the energy contribution in ultraviolet in our old and metal-rich models without blue horizontal branch (HB) for an He-normal population. If one compares to the blue HB formed from He-rich stars (Fig. 2), it is expected that the low number of BSs usually present in GCs (Piotto et al. 2004) would lead only to a small contribution in the ultraviolet band. Thus, it is important to keep in mind that BSs will change the properties of our He-normal population in the ultraviolet band. Post-AGB stars dominate the energy contribution only in the far-UV ($\lesssim$2000 Å; Chung et al. 2017) at the ages and metallicities investigated in this paper. Finally Hernández-Pérez & Bruzual (2014) showed that interacting binaries might form extreme HB stars and in turn lead to strong emissions in the ultraviolet band, providing an alternative solution to explain the UV-upturn phenomenon in ETGs. The binary fraction required then is at least 15 per cent, which is relatively similar to what is found in low-metallicity Galactic GCs (see Milone et al. 2012). Thus, BSs and post-AGB stars do not affect the conclusions of our study. However,

Downloaded from https://academic.oup.com/mnras/article-abstract/478/2/2368/4995915
by Liverpool John Moores University user
on 10 July 2018

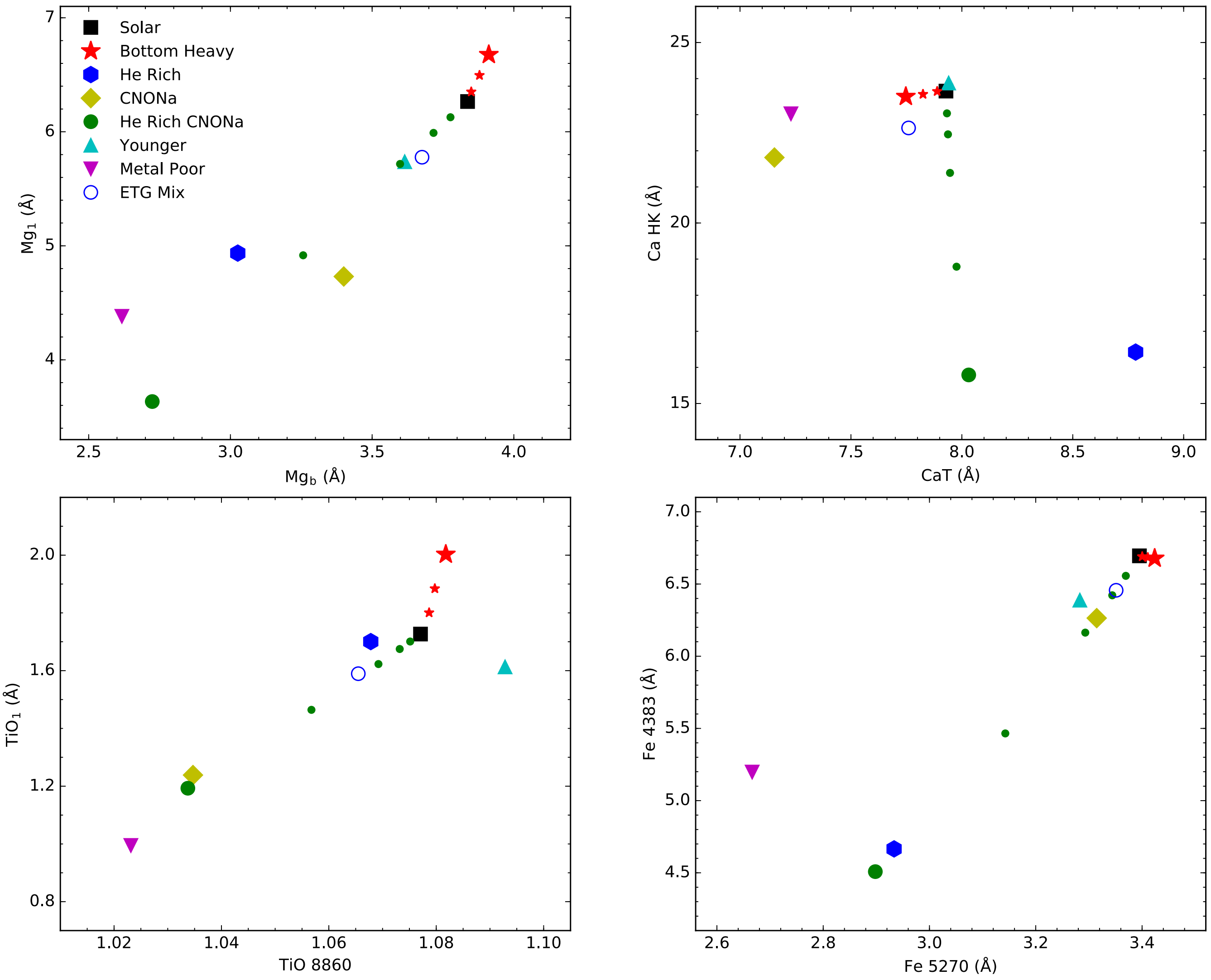

**Figure 10.** Line index strengths. The symbol shapes and colours are as in Fig. 6. *Top left:* $Mg_1$ MgH molecular band strength versus $Mg_b$ line index. While the bottom heavy IMF displays stronger $Mg_1$ and $Mg_b$ strengths, the He-rich model shows weaker $Mg_1$, $Mg_b$. The CNONa mixture leads to weaker Mg index strengths. *Top right:* Strength of the Ca H and K lines versus the strength of the calcium triplet (CaT). While the bottom heavy IMF model shows weaker CaT strength, similar H and K strengths with respect to the solar composition, Kroupa IMF model, the He-rich model shows significantly weaker H and K absorption and stronger CaT absorption. The stronger CaT index strengths in the He-rich model are due to contamination by the stronger Paschen line absorption in the He-rich model (see Fig. 9). The CNONa mixture leads to weaker Ca index strengths. *Bottom left:* Effects of He abundance on the $TiO_1$ and TiO 8860 TiO molecular indices. Whereas the bottom heavy IMF model shows stronger $TiO_1$ and marginally stronger TiO 8860 band strengths, the He-rich model shows weaker TiO 8860 absorption and no change in the $TiO_1$ index. The low O abundance second-population abundance pattern models show weaker TiO band strengths with respect to the models with solar [O/Fe]. *Bottom right:* Effects of He on the Fe 4383 and Fe 5270 indices. While the IMF has little effect on the strength of these Fe absorption indices, increased He abundance produces weaker index strengths as does the CNONa mixture. The effect of enhanced He instead resembles the effects of a younger age.

it would be interesting to include binaries in future studies and to couple them with He-rich models in order to be more consistent when studying the UV contribution.

As we have shown in this study, the He-rich population has a non-negligible effect on mass of the stars still in the nuclear active phase but also the remnants when considered separately (for the extreme case $Y_{\rm ini}= 0.4$). However, the effect becomes negligible when one looks at the total mass of the population. Thus, in studies where the mass of remnants or stars plays a crucial role, it is more consistent to take into account suitable initial-final mass relations and mass cut-off (minimum $M_{\rm ini}$ for remnants) for the He-rich population. In addition, for this extreme He content, it would be interesting to know for stars which do not end their life as WDs if their final masses and mass boundaries change. For instance, as shown in this study and pointed out in Shingles et al. (2015), the He enhancement will increase the formation rate of NSs through electron-capture supernovae.

We have shown that from the theoretical point of view, the optical *M*/*L* of both He-rich and He-normal populations is similar. Then to observationally highlight the presence of an He-rich population at work in ETGs through *M*/*L*, it is mandatory to focus on shorter wavelengths. The effects of the He-rich population are already seen at ∼4000 Å and ∼2600 Å (if we compare to populations with $Y_{\rm ini}= 0.4$ and the ETG mixture, respectively). Note that we have

Downloaded from https://academic.oup.com/mnras/article-abstract/478/2/2368/4995915
by Liverpool John Moores University user
on 10 July 2018

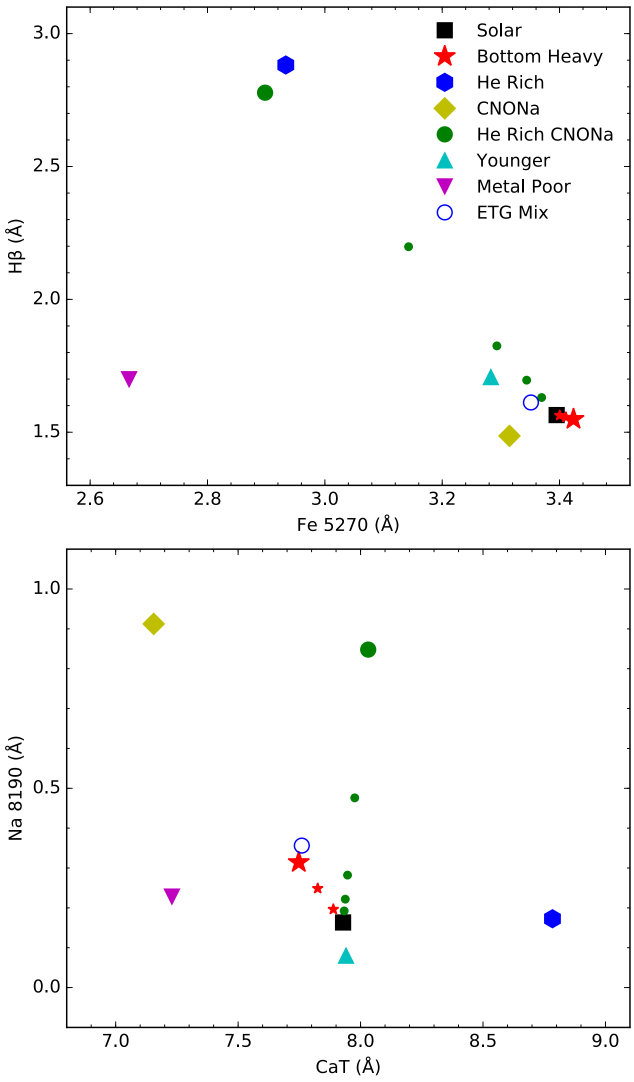

**Figure 11.** Line index strengths. The symbol shapes and colours are as in Fig. 6. *Top:* Strength of H$\beta$ versus the Fe 5270 spectral index. The He-rich models have significantly stronger H$\beta$ and weaker Fe 5270 index strengths with respect to the solar composition model making them appear like a younger population rather than a bottom heavy IMF which shows marginally stronger Fe 5270 strength. The CNONa model has weaker H$\beta$ and Fe 5270 indices. *Bottom:* Strength of the Na 8190 index versus the CaT spectral index. The He-rich solar model has stronger CaT values due to stronger Paschen lines while the CNONa model has stronger Na 8190 and weaker CaT strengths mimicking a bottom heavy IMF.

to be careful since an He-rich population mimic the $M/L$ of an He-normal population at lower metallicity and/or younger age in $U$ bands.

## 8 CONCLUSION

Massive ETGs display radial abundance gradients which do not correspond to standard chemical predictions and $M/L$ variations which might be explained so far only with a debated change in the stellar IMF. Since multiple stellar populations of GCs display similar chemical trends and are expected to lead to $M/L$ variations, we investigate in this paper if these multiple stellar populations could be the source of these patterns observed in their host galaxies.

We use a toy model to estimate the contribution of disrupted GCs to the centres of massive ETGs. We find that ~35 per cent of stars in a massive ETG should show the N, Na-enhanced, C, O depleted chemistry of second population GC stars. This contribution of GC stars can explain the Na-enriched, O and C depleted abundance pattern seen in the centres of massive ETGs (van Dokkum et al. 2017). We also estimate that ~5 per cent of stars should show extreme He enhancement ($\Delta Y > 0.1$).

We have constructed single stellar population models with a range of He abundances, chemistries, and IMFs. For each of our model of spectral energy distribution, we calculate synthetic magnitudes and spectral indices. We consider the effects of helium abundance on stellar final masses allowing us to study the effects of helium on the mass-to-light ratio.

We find that the lower mass in nuclear burning stars in an He-rich population is largely offset by the higher total mass locked into the remnants. As such, the lower $M/L$ of an He-rich population is due to its higher luminosity. Since changes in abundance pattern at fixed C+N+O have little effect on stellar evolution and since differences in the abundance pattern have little effect on broad-band magnitudes, the N, Na-enhanced, C, O depleted models have quite similar $M/L$ ratios to models with the same He abundance.

Both the colours and the spectral indices of He-rich populations resemble a younger population rather than a bottom heavy IMF. However, a N, Na-enhanced, C, O depleted population can mimic the effects of a bottom heavy IMF on some IMF spectral indices (Na D, Na 8190, CaT) but not others (such as TiO bands).

We also find that the small contribution of He-rich stars of our toy model (stars with $\Delta Y > 0.1$) has little effect on the spectral energy distribution redwards of 4000 Å but is enough to dramatically change the flux bluewards of 2600 Å contributing to the UV-upturn phenomenon.

We conclude that He enhancement cannot mimic the observational signatures of a bottom heavy IMF as an He-rich population resembles as younger population instead. However, we find disrupted GCs can supply a significant number of He, N, and Na enhanced, C and O depleted stars to the field star population of massive ETGs. These stars can at least partially explain the UV-excess and the chemistry of the centres of massive ETGs. A similar conclusion was recently reached by Goudfrooij (2018), who studied the correlation between the UV-upturn strength and the specific frequency (the number of GCs per unit galaxy light) in early-type galaxies.

More detailed stellar population modelling is required to compare the predictions of this work with the observed spectra of the centres of massive ETGs. In a future work (Schiavon et al. in preparation), we will quantitatively explore the abundance gradients in ETGs and match them to the variations observed in GCs due to multiple populations.

## ACKNOWLEDGEMENTS

We warmly thank J. Pfeffer for useful discussions and M. Salaris and R. Schiavon for careful reading and useful comments on the manuscript. W. Chantereau acknowledges funding from the Swiss National Science Foundation under grant P2GEP2_171971 and thanks the International Space Science Institute (ISSI, Bern, CH) for welcoming the activities of the Team 271 ‘Massive Star Clusters Across the Hubble Time’. C.U. and N.B. gratefully acknowledge financial support from the European Research Council (ERC-CoG-646928, Multi-Pop). N.B. gratefully acknowledges financial support from the Royal Society (University Research Fellowship).

Downloaded from https://academic.oup.com/mnras/article-abstract/478/2/2368/4995915
by Liverpool John Moores University user
on 10 July 2018

This work made use of the PYTHON packages NUMPY (van der Walt, Colbert & Varoquaux 2011), SCIPY (Jones et al. 2001), and MATPLOTLIB (Hunter 2007) as well as ASTROPY, a community-developed core PYTHON package for astronomy (Astropy Collaboration 2013).

## REFERENCES

Althaus L. G., De Gerónimo F., Córsico A., Torres S., García-Berro E., 2017, A&A, 597, A67

Asplund M., 2005, ARA&A, 43, 481

Asplund M., Grevesse N., Sauval A. J., Scott P., 2009, ARA&A, 47, 481

Astropy Collaboration, 2013, A&A, 558, A33

Baraffe I., Chabrier G., Allard F., Hauschildt P. H., 1998, A&A, 337, 403

Bastian N., 2008, MNRAS, 390, 759

Bastian N., Lardo C., 2017, preprint (arXiv:1712.01286)

Bastian N., Saglia R. P., Goudfrooij P., Kissler-Patig M., Maraston C., Schweizer F., Zoccali M., 2006, A&A, 448, 881

Bastian N.  et al., 2012, MNRAS, 419, 2606

Behr B. B., 2003, ApJS, 149, 67

Belczynski K., Bulik T., Fryer C. L., Ruiter A., Valsecchi F., Vink J. S., Hurley J. R., 2010, ApJ, 714, 1217

Bellini A.  et al., 2015, ApJ, 805, 178

Bertelli G., Girardi L., Marigo P., Nasi E., 2008, A&A, 484, 815

Bird S., Harris W. E., Blakeslee J. P., Flynn C., 2010, A&A, 524, A71

Brown J. A., Wallerstein G., Oke J. B., 1991, AJ, 101, 1693

Brown T. M., Ferguson H. C., Davidsen A. F., Dorman B., 1997, ApJ, 482, 685

Brown T. M., Bowers C. W., Kimble R. A., Sweigart A. V., Ferguson H. C., 2000, ApJ, 532, 308

Bruzual G., Charlot S., 2003, MNRAS, 344, 1000

Burstein D., Bertola F., Buson L. M., Faber S. M., Lauer T. R., 1988, ApJ, 328, 440

Busso G.  et al., 2007, A&A, 474, 105

Cappellari M.  et al., 2012, Nature, 484, 485

Carretta E., Cohen J. G., Gratton R. G., Behr B. B., 2001, AJ, 122, 1469

Carretta E.  et al., 2009a, A&A, 505, 117

Carretta E., Bragaglia A., Gratton R., Lucatello S., 2009b, A&A, 505, 139

Carretta E., Bragaglia A., Gratton R. G., Recio-Blanco A., Lucatello S., D'Orazi V., Cassisi S., 2010, A&A, 516, A55

Cassisi S., Mucciarelli A., Pietrinferni A., Salaris M., Ferguson J., 2013, A&A, 554, A19

Cassisi S., Salaris M., Pietrinferni A., Vink J. S., Monelli M., 2014, A&A, 571, A81

Catelan M., Valcarce A. A. R., Sweigart A. V., 2010, in de Grijs R., Lépine J. R. D., eds, IAU Symp. 266, Star Clusters: Basic Galactic Building Blocks Throughout Time and Space. p. 281 (arXiv:0910.1367)

Cenarro A. J., Cardiel N., Gorgas J., Peletier R. F., Vazdekis A., Prada F., 2001, MNRAS, 326, 959

Chabrier G., Baraffe I., 1997, A&A, 327, 1039

Chantereau W., Charbonnel C., Decressin T., 2015, A&A, 578, A117

Chantereau W., Charbonnel C., Meynet G., 2016, A&A, 592, A111

Chantereau W., Charbonnel C., Meynet G., 2017, A&A, 602, A13

Charbonnel C., 2016, in Moraux E., Lebreton Y., Charbonnel C., eds, EAS Publications Series Vol. 80, EAS Publications Series. p. 177 (arXiv:1611.08855)

Charbonnel C., Chantereau W., 2016, A&A, 586, A21

Chung C., Lee S.-Y., Yoon S.-J., Lee Y.-W., 2013, ApJ, 769, L3

Chung C., Yoon S.-J., Lee Y.-W., 2017, ApJ, 842, 91

Code A. D., Welch G. A., 1979, ApJ, 228, 95

Coelho P., Percival S. M., Salaris M., 2011, ApJ, 734, 72

Cohen J. G., Meléndez J., 2005, AJ, 129, 303

Conroy C., van Dokkum P., 2012a, ApJ, 747, 69

Conroy C., van Dokkum P. G., 2012b, ApJ, 760, 71

Conroy C., Gunn J. E., White M., 2009, ApJ, 699, 486

Conroy C., Graves G. J., van Dokkum P. G., 2014, ApJ, 780, 33

Conroy C., Villaume A., van Dokkum P. G., Lind K., 2018, ApJ, 854, 139

D'Antona F., Caloi V., Ventura P., 2010, MNRAS, 405, 2295

Dalessandro E., Schiavon R. P., Rood R. T., Ferraro F. R., Sohn S. T., Lanzoni B., O'Connell R. W., 2012, AJ, 144, 126

Denisenkov P. A., Denisenkova S. N., 1990, Sov. Astron. Lett., 16, 275

Di Criscienzo M., Tailo M., Milone A. P., D'Antona F., Ventura P., Dotter A., Brocato E., 2015, MNRAS, 446, 1469

Dickens R. J., Croke B. F. W., Cannon R. D., Bell R. A., 1991, Nature, 351, 212

Donas J.  et al., 2007, ApJS, 173, 597

Dorman B., O'Connell R. W., Rood R. T., 1995, ApJ, 442, 105

Dotter A., Chaboyer B., Jevremović D., Baron E., Ferguson J. W., Sarajedini A., Anderson J., 2007, AJ, 134, 376

Forbes D. A., Sánchez-Blázquez P., Phan A. T. T., Brodie J. P., Strader J., Spitler L., 2006, MNRAS, 366, 1230

Gallazzi A., Charlot S., Brinchmann J., White S. D. M., Tremonti C. A., 2005, MNRAS, 362, 41

Gallazzi A., Charlot S., Brinchmann J., White S. D. M., 2006, MNRAS, 370, 1106

Gieles M., Larsen S. S., Bastian N., Stein I. T., 2006, A&A, 450, 129

Goudfrooij P., 2018, ApJ, 857, 16

Goudfrooij P., Gilmore D., Whitmore B. C., Schweizer F., 2004, ApJ, 613, L121

Gratton R. G., Carretta E., Bragaglia A., 2012, A&A Rev., 20, 50

Graves G. J., Schiavon R. P., 2008, ApJS, 177, 446

Greggio L., Renzini A., 1990, ApJ, 364, 35

Harris W. E., 1996, AJ, 112, 1487

Harris W. E., Harris G. L. H., 2002, AJ, 123, 3108

Harris W. E., Harris G. L. H., Alessi M., 2013, ApJ, 772, 82

Heavens A., Panter B., Jimenez R., Dunlop J., 2004, Nature, 428, 625

Hernández-Pérez F., Bruzual G., 2014, MNRAS, 444, 2571

Hunter J. D., 2007, Comput. Sci. Eng., 9, 90

Ivans I. I., Sneden C., Kraft R. P., Suntzeff N. B., Smith V. V., Langer G. E., Fulbright J. P., 1999, AJ, 118, 1273

Johansson J., Thomas D., Maraston C., 2012, MNRAS, 421, 1908

Johnson C. I., Rich R. M., Kobayashi C., Kunder A., Koch A., 2014, AJ, 148, 67

Johnson L. C.  et al., 2017, ApJ, 839, 78

Jones E., Oliphant T., Peterson P.  et al., 2001, SciPy: Open source scientific tools for Python, http://www.scipy.org/

Kamath D., Karakas A. I., Wood P. R., 2012, ApJ, 746, 20

Karakas A. I., 2014, MNRAS, 445, 347

King I. R.  et al., 2012, AJ, 144, 5

Kotulla R., Fritze U., Weilbacher P., Anders P., 2009, MNRAS, 396, 462

Kroupa P., 2001, MNRAS, 322, 231

Kruijssen J. M. D., 2014, Class. Quant. Gravity, 31, 244006

Kruijssen J. M. D., 2015, MNRAS, 454, 1658

Kurucz R. L., 1970, SAO Spec. Rep., 309

Kurucz R. L., 2005, Memorie della Soc. Astron. Italiana Suppl., 8, 14

Kurucz R. L., Avrett E. H., 1981, SAO Spec. Rep., 391

Kurucz R. L., Furenlid I., 1979, SAO Spec. Rep., 387

La Barbera F., Ferreras I., Vazdekis A., de la Rosa I. G., de Carvalho R. R., Trevisan M., Falcón-Barroso J., Ricciardelli E., 2013, MNRAS, 433, 3017

La Barbera F., Vazdekis A., Ferreras I., Pasquali A., Allende Prieto C., Röck B., Aguado D. S., Peletier R. F., 2017, MNRAS, 464, 3597

Lagioia E. P.  et al., 2014, ApJ, 782, 50

Larsen S. S., 2009, A&A, 494, 539

Maraston C., 1998, MNRAS, 300, 872

Maraston C., Greggio L., Renzini A., Ortolani S., Saglia R. P., Puzia T. H., Kissler-Patig M., 2003, A&A, 400, 823

Maraston C., Bastian N., Saglia R. P., Kissler-Patig M., Schweizer F., Goudfrooij P., 2004, A&A, 416, 467

Marigo P., Girardi L., Bressan A., Groenewegen M. A. T., Silva L., Granato G. L., 2008, A&A, 482, 883

Martell S. L., Grebel E. K., 2010, A&A, 519, A14

Martell S. L.  et al., 2016, ApJ, 825, 146

Martocchia S.  et al., 2017, MNRAS, 468, 3150

Martocchia S.  et al., 2018, MNRAS, 473, 2688

Matteucci F., 1994, A&A, 288, 57

McDermid R. M.  et al., 2015, MNRAS, 448, 3484

Downloaded from https://academic.oup.com/mnras/article-abstract/478/2/2368/4995915
by Liverpool John Moores University user
on 10 July 2018

McLaughlin D. E., 1999, AJ, 117, 2398
Milone A. P., 2015, MNRAS, 446, 1672
Milone A. P. et al., 2012, A&A, 540, A16
Milone A. P. et al., 2015, ApJ, 808, 51
Milone A. P. et al., 2017, MNRAS, 464, 3636
Norris J. E., Da Costa G. S., 1995, ApJ, 447, 680
O'Connell R. W., 1999, ARA&A, 37, 603
Pace G., Recio-Blanco A., Piotto G., Momany Y., 2006, A&A, 452, 493
Panter B., Jimenez R., Heavens A. F., Charlot S., 2007, MNRAS, 378, 1550
Peng F., Nagai D., 2009, ApJ, 705, L58
Peng E. W. et al., 2006, ApJ, 639, 95
Peng E. W. et al., 2008, ApJ, 681, 197
Pfeffer J., Kruijssen J. M. D., Crain R. A., Bastian N., 2018, MNRAS, 475, 4309
Pietrinferni A., Cassisi S., Salaris M., Percival S., Ferguson J. W., 2009, ApJ, 697, 275
Piotto G., 2009, in Mamajek E. E., Soderblom D. R., Wyse R. F. G., eds, IAU Symp. 258, The Ages of Stars. p. 233
Piotto G. et al., 2004, ApJ, 604, L109
Ramírez I., Meléndez J., Chanamé J., 2012, ApJ, 757, 164
Renzini A., Ciotti L., 1993, ApJ, 416, L49
Rey S.-C. et al., 2009, ApJ, 700, L11
Salaris M., Weiss A., Ferguson J. W., Fusilier D. J., 2006, ApJ, 645, 1131
Salpeter E. E., 1955, ApJ, 121, 161
Sarzi M., Spiniello C., La Barbera F., Krajnović D., van den Bosch R., 2017, preprint (arXiv:1711.08980)
Sbordone L., Salaris M., Weiss A., Cassisi S., 2011, A&A, 534, A9
Schiavon R. P., 2007, ApJS, 171, 146
Schiavon R. P., Rose J. A., Courteau S., MacArthur L. A., 2004, ApJ, 608, L33
Schiavon R. P., Caldwell N., Conroy C., Graves G. J., Strader J., MacArthur L. A., Courteau S., Harding P., 2013, ApJ, 776, L7
Schiavon R. P. et al., 2017a, MNRAS, 465, 501
Schiavon R. P. et al., 2017b, MNRAS, 466, 1010
Serven J., Worthey G., Briley M. M., 2005, ApJ, 627, 754
Shingles L. J., Doherty C. L., Karakas A. I., Stancliffe R. J., Lattanzio J. C., Lugaro M., 2015, MNRAS, 452, 2804
Short C. I., Young M. E., Layden N., 2015, ApJ, 810, 76
Smith G. H., Shetrone M. D., Bell R. A., Churchill C. W., Briley M. M., 1996, AJ, 112, 1511
Sohn S. T., O'Connell R. W., Kundu A., Landsman W. B., Burstein D., Bohlin R. C., Frogel J. A., Rose J. A., 2006, AJ, 131, 866
Spiesman W. J., 1992, ApJ, 397, L103
Strader J. et al., 2013, ApJ, 775, L6
Tailo M., Di Criscienzo M., D'Antona F., Caloi V., Ventura P., 2016, MNRAS, 457, 4525
Tang B., Worthey G., Davis A. B., 2014, MNRAS, 445, 1538
Tang B. et al., 2017, MNRAS, 465, 19
Thomas D., Maraston C., Bender R., 2003, MNRAS, 339, 897
Thomas D., Maraston C., Bender R., Mendes de Oliveira C., 2005, ApJ, 621, 673
Trager S. C., Faber S. M., Worthey G., González J. J., 2000, AJ, 120, 165
Usher C. et al., 2012, MNRAS, 426, 1475
Usher C. et al., 2017, MNRAS, 468, 3828
Valcarce A. A. R., Catelan M., Sweigart A. V., 2012, A&A, 547, A5
van der Walt S., Colbert S. C., Varoquaux G., 2011, Comp. Sci. Eng., 13, 22
van Dokkum P. G., Conroy C., 2010, Nature, 468, 940
van Dokkum P. G., Conroy C., 2014, ApJ, 797, 56
van Dokkum P., Conroy C., Villaume A., Brodie J., Romanowsky A. J., 2017, ApJ, 841, 68
Wachter A., Schröder K.-P., Winters J. M., Arndt T. U., Sedlmayr E., 2002, A&A, 384, 452
Wedemeyer S., Kucinskas A., Klevas J., Ludwig H.-G., 2017, A&A, 606, 26
Whitmore B. C., Zhang Q., Leitherer C., Fall S. M., Schweizer F., Miller B. W., 1999, AJ, 118, 1551
Worthey G., 1994, ApJS, 95, 107
Worthey G., Ottaviani D. L., 1997, ApJS, 111, 377
Worthey G., Faber S. M., Gonzalez J. J., 1992, ApJ, 398, 69
Worthey G., Faber S. M., Gonzalez J. J., Burstein D., 1994, ApJS, 94, 687
Worthey G., Tang B., Serven J., 2014, ApJ, 783, 20
Yi S., Demarque P., Oemler Jr. A., 1997, ApJ, 486, 201
Yi S. K., Lee J., Sheen Y.-K., Jeong H., Suh H., Oh K., 2011, ApJS, 195, 22
Yong D., Grundahl F., Norris J. E., 2015, MNRAS, 446, 3319
Zaritsky D., Gil de Paz A., Bouquin A. Y. K., 2015, MNRAS, 446, 2030
Zoccali M., Renzini A., Ortolani S., Bica E., Barbuy B., 2001, AJ, 121, 2638
Zoccali M. et al., 2004, A&A, 423, 507

## APPENDIX A: A COMPARISON WITH THE CONROY & VAN DOKKUM (2012) MODELS

To assess the reliability of our stellar population models, we compared the colours, spectral indices, and *M*/*L* predicted by our models

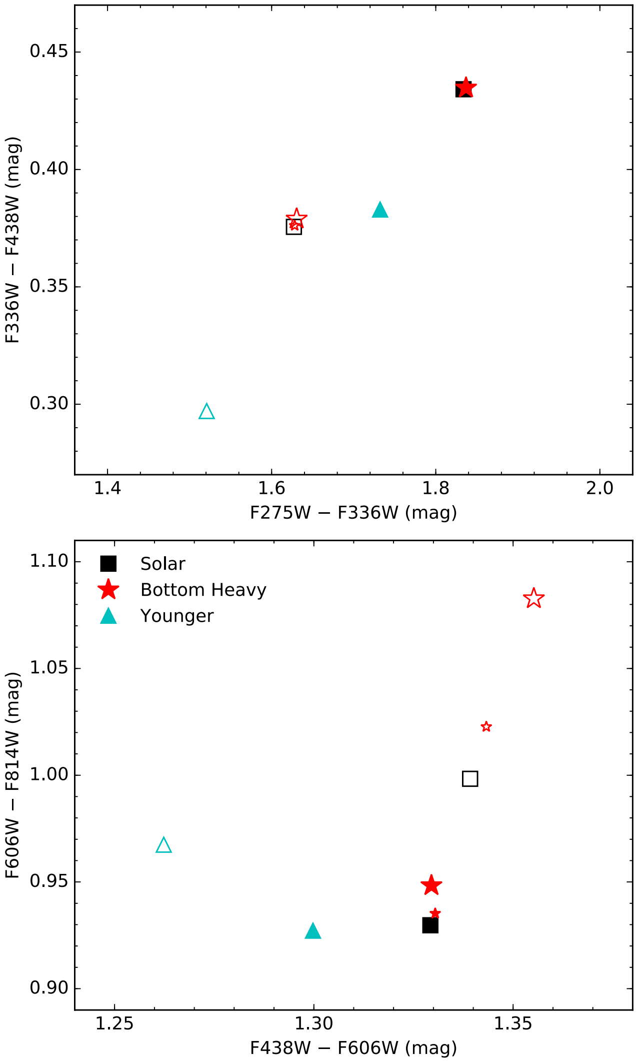

**Figure A1.** Comparison of the predicted colours for our models (solid points) with the predictions of the models of Conroy & van Dokkum (2012a) (open points). As in Fig. 6, the black squares are models with solar abundances and a Milky Way like IMF, the red stars are solar composition models with bottom heavy IMFs and the cyan triangles are the younger (8.9 Gyr) models. While the colours plotted are the same as in Fig. 6, the axes ranges are different. Although the colours of the Conroy models are bluer in the bluer bands (top) and redder in the redder bands (bottom) than our models, the effects of a younger age or a bottom heavy IMF are broadly similar for both models although a bottom heavy IMF has a much larger effect on the (F606W–F814W) colour of the Conroy models than for our models.

Downloaded from https://academic.oup.com/mnras/article-abstract/478/2/2368/4995915
by Liverpool John Moores University user
on 10 July 2018

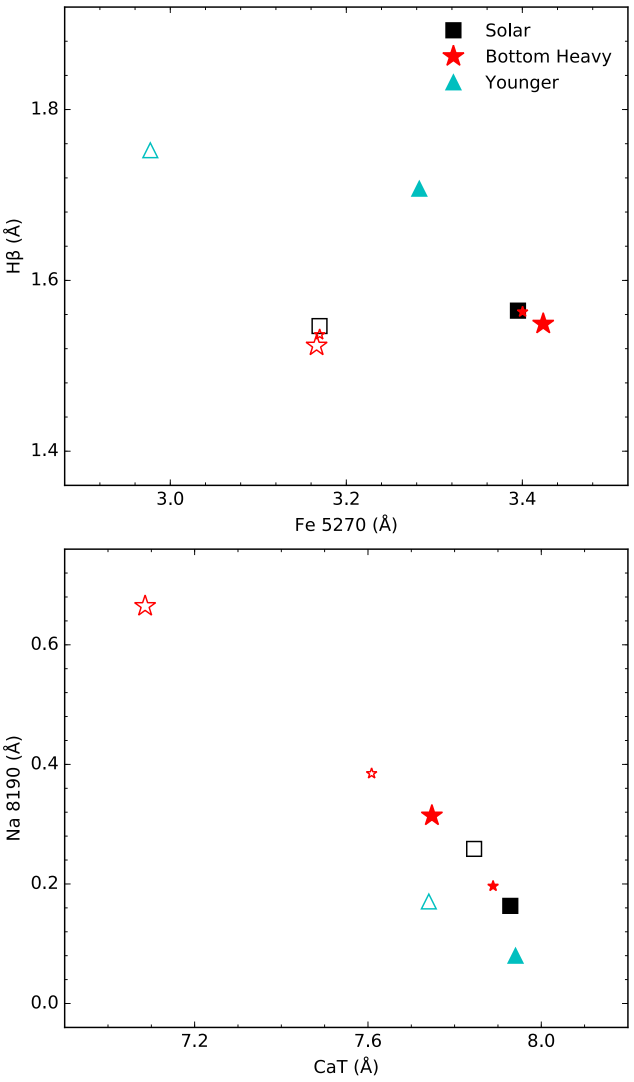

**Figure A2.** Comparison of the predicted spectral indices for our models (solid points) with the predictions of the models of Conroy & van Dokkum (2012a) (open points). The colours and shapes of the points are the same as in Fig. A1. While the colours plotted are the same as in Fig. 11, the axes ranges are different. While there are differences in index values between our models and the Conroy models, both sets of models show similar behaviour although the Conroy models show larger IMF effects.

with those of Conroy & van Dokkum (2012a). We downloaded version 1.2 of the Conroy & van Dokkum spectral energy distributions and after smoothing them to match the velocity dispersion of our models, we performed the same magnitude and spectral index measurements as we did for our models (Section 3.3). To calculate mass-to-light ratios for the Conroy models, we used their initial-to-final mass relations. We are able to make a comparison with equivalent models for our base solar composition, Milky Way-like IMF model, our bottom heavy IMF ($\alpha = -3$) model, our Salpeter IMF model, and our young model. We cannot compare our lower metallicity model with the Conroy models as only models where a single element is varied are publicly available. Likewise, we cannot directly compare our CNONa models to any of the Conroy models with variations of a single element due to the complex interdependence of the abundance of different atomic and molecular species on each other. However, a visual comparison of our Figs 9 and 10 with the figures in Conroy & van Dokkum (2012a) does generally show qualitative agreement for the effects of changing the dominant element of an index. We note that we vary the abundances of each of C, N, O, and Na by larger amounts than do Conroy & van Dokkum (2012a) and that the effects of [N/Fe] dominate the effects of [C/Fe] on the $\mathrm{CN_1}$ index.

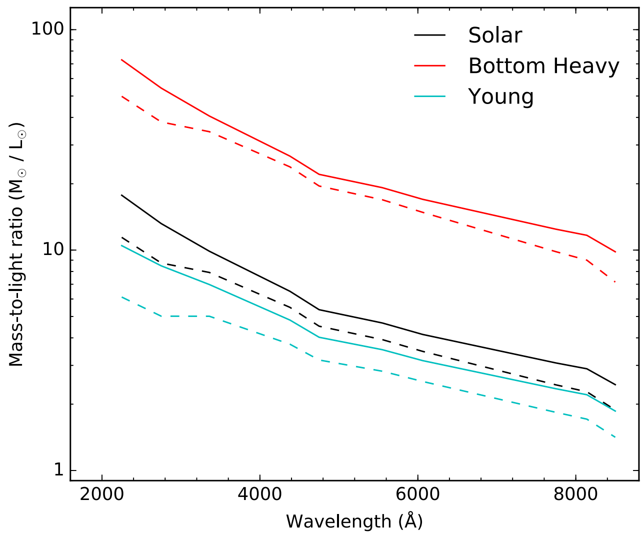

**Figure A3.** Comparison of the predicted *M*/*L* for our models (solid lines) with the predictions of the models of Conroy & van Dokkum (2012a) (dashed lines). The colours of the lines are the same as in Fig. A1. Other than a 0.1 dex offset, there is good agreement between the two sets of models.

We plot a comparison of the colours predicted by the two sets of models in Fig. A1, a comparison of a subset of the spectral indices in Fig. A2 and a comparison of the predicted *M*/*L* in Fig. A3. While we do see zero-point offsets between our models and those of Conroy & van Dokkum (2012a), we generally see similar qualitative behaviour with age and the IMF for both sets of models. Both sets of models predict bluer colours for younger ages although there are differences in the size of the colour effect for the redder colours. While both sets of models predict little effect of the IMF on the bluer colours, the Conroy & van Dokkum (2012a) models predict a much larger effect of a bottom heavy IMF on redder colours in the bottom of Fig. A1. In H$\beta$–Fe 5270 space, both sets of models display similar behaviour with age (stronger H$\beta$, weaker Fe 5270 indices) and with a bottom heavy IMF (little effect on either H$\beta$ or Fe 5270). In Na 8190-CaT space, both models predict stronger Na 8190 indices and weaker CaT indices for a bottom heavy IMF compared to a Kroupa IMF although the Conroy & van Dokkum (2012a) models predict a much larger effect. Both models predict weaker Na 8190 indices at younger ages, but the Conroy & van Dokkum (2012a) models predict a slightly weaker CaT at younger ages while our models predict no effect of age on the CaT. Modulo a 0.1 dex offset between our models and the Conroy models, we see excellent agreement in the *M*/*L* predictions.

The differences between our models and those of Conroy & van Dokkum (2012a) are not surprising given that we use synthetic spectra where the Conroy models use empirical spectral libraries supplemented by synthetic spectra. Differences in the sizes of the effect of changing IMF between the two sets of models are likely due to lower mass stars. The lowest mass stellar model we compute is a 3200 K 0.12 $\mathrm{M_\odot}$ star – the lowest mass point in the Dotter et al. (2007) isochrones – while the Conroy models include empirical spectra of stars as cool as 2200 K and as low mass as 0.08 $\mathrm{M_\odot}$.

Downloaded from https://academic.oup.com/mnras/article-abstract/478/2/2368/4995915
by Liverpool John Moores University user
on 10 July 2018

Although both sets of models are based on similar isochrones for stars more massive than 0.17 $M_\odot$ (Dotter et al. 2007 isochrones for the MS and RGB; Padova isochrones Marigo et al. 2008; Bertelli et al. 2008 for the post-RGB evolution), the Conroy models utilize the Lyon isochrones (Chabrier & Baraffe 1997; Baraffe et al. 1998) for the lowest mass stars. As our models are intended to allow us to explore the differential effects of various abundance patterns and IMF and not to replicate observations, we consider the similar qualitative behaviour of our models to those of Conroy & van Dokkum (2012a) to be sufficient for our purposes.

## APPENDIX B: A COMPARISON WITH THE METAL-RICH GLOBULAR CLUSTERS NGC 6528 AND NGC 6553

To test our models, we compared our predicted indices with those measured on the observed spectra of the metal rich Milky Way GCs NGC 6528 and NGC 6553. Both NGC 6528 and NGC 6553 are old (11–13 Gyr, e.g. Zoccali et al. 2001; Lagioia et al. 2014) and have slightly subsolar metallicities ([Fe/H] = −0.11 and −0.18, respectively, 2010 edition of the Harris 1996 catalogue). These GCs show slight $\alpha$-element enhancements and the light element abundance anticorrelations characteristic of multiple populations in GCs (e.g. Carretta et al. 2001; Zoccali et al. 2004; Johnson et al. 2014; Schiavon et al. 2017b). We use publicly available spectra from the WAGGS project (Usher et al. 2017) that cover the wavelength range of 3300–9050 Å at a resolution of $R \sim 6800$. As was done for the Conroy & van Dokkum models, we smoothed the observed spectra to match the velocity dispersion of our models and we performed the same spectral index measurements as we did for our models (Section 3.3).

We plot a comparison of our model predictions with the indices measured on the observed spectra of NGC 6528 and NGC 6553 in Figs B1 and B2. Given the similar ages, metallicities, and chemistries of the two observed GCs, the differences in measured indices provide a rough measure of the uncertainty of the index measurements. For the Balmer indices and the Fe indices, the observations lie close to our metal poor model ([Fe/H]=−0.3) that is unsurprising, given their slightly subsolar [Fe/H] abundances. The observed Mg indices are slightly weaker than our base solar metallicity model that is consistent with the GCs being having a subsolar [Fe/H] but slightly supersolar [Mg/Fe]. Given the large observational uncertainties on the Ca H and K lines, our models are broadly consistent with near solar [Ca/H] GCs. The observed CH 4300 bands are weaker than our solar metallicity model but the $CN_1$ bands are stronger than the model. This is consistent with both the C-N anticorrelation observed in these GCs and the effects of the first dredge-up that are not included in our models. Our C depleted, N enhanced models predict the observed $CN_1$ strengths but underpredicts the CH 4300 abundances. Likewise, we measure stronger Na D strengths than predicted by our solar abundance model but are consistent with enhanced [Na/Fe] ratios. We note that interstellar Na D absorption can increase the observed Na D, especially for GCs with significant foreground extinction such as NGC 6528 and NGC 6553.

Perhaps unsurprisingly, our models do not predict the observed TiO band strengths with the spectra of the two GCs showing wildly different TiO strengths. Observationally, the TiO band strengths are the spectral features most effected by stochastic effects as they are mostly produced by the brightest, coolest giants (van Dokkum & Conroy 2014; Usher et al. 2017). Our spectral synthesis is least reliable for such cool, low surface gravity stars. The strong TiO bands affect a number of the spectral features we consider in the red. The red continuum passband for the Na 8190 index overlaps with a TiO bandhead, so the stronger observed TiO absorption leads to a weaker Na 8190 strength. The wavelength region covered by the CaT and PaT indices is also affected by TiO bands with stronger TiO bands weakly lowering the observe CaT strength but strongly lowering the PaT strength. Due to the sensitivity of some of the indices on TiO, we do include these bands in our comparison.

Given the statistical and systematic uncertainties both in the observed spectra and in the literature metallicities and abundances, and the limitations of our modelling, we consider our models to be in agreement with observations. We remind the reader that our models were designed to allow us to study the differential effects of various chemical mixtures and IMFs and were not intended to replicate observations in detail.

Downloaded from https://academic.oup.com/mnras/article-abstract/478/2/2368/4995915
by Liverpool John Moores University user
on 10 July 2018

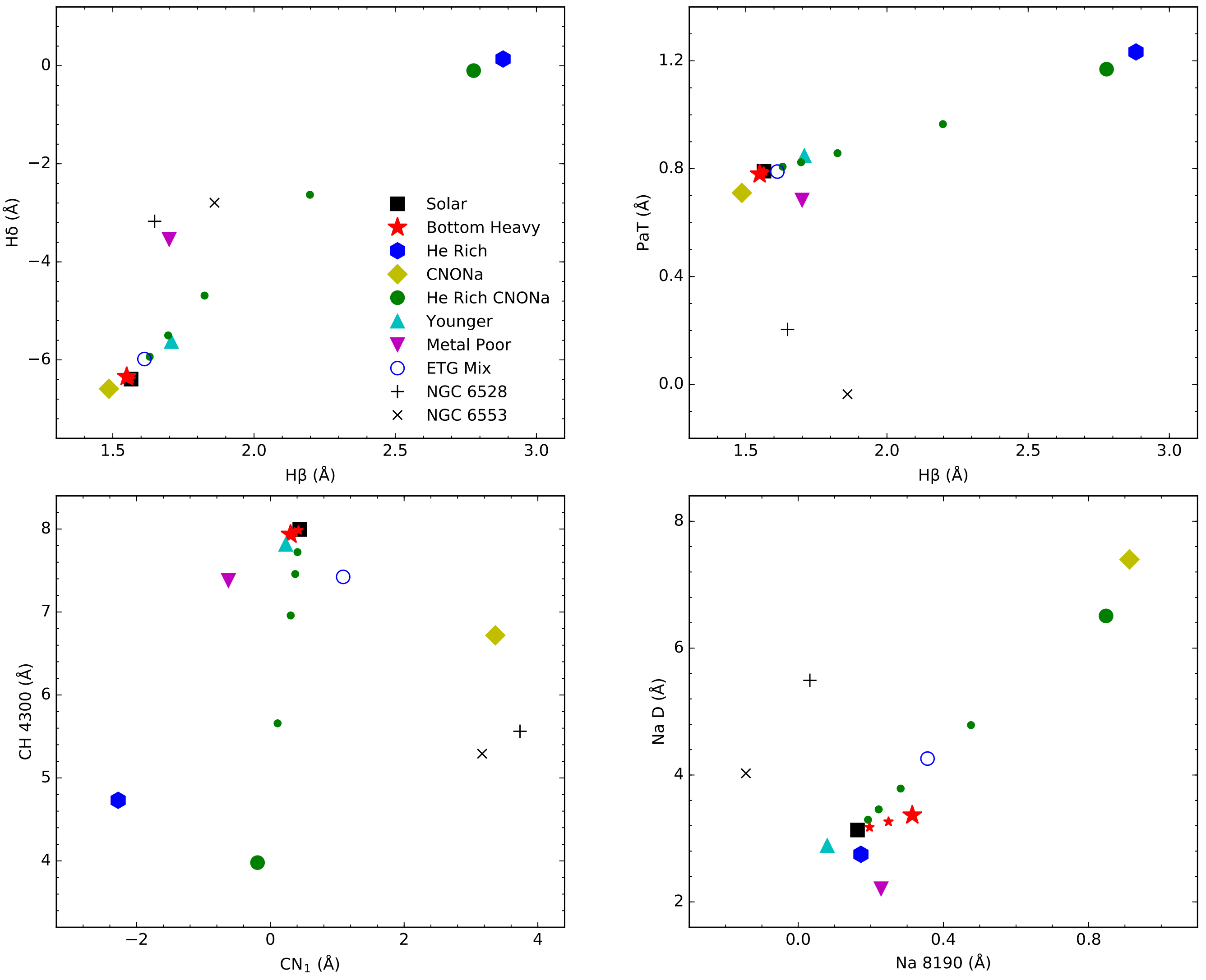

**Figure B1.** Comparison of model line index strengths with observations. The model symbol shapes and colours are as in Fig. 6 while the GCs NGC 6528 and NGC 6553 are represented by a black plus and x markers, respectively. *Top left:* Strength of the Hδ line index versus the strength of the Hβ line index. *Top right:* Strength of PaT Paschen line index versus the strength of the Hβ line index. *Bottom left:* Strength of the CH 4300 molecular index versus the strength of the $CN_1$ molecular index. *Bottom right:* the Na D and Na 8190 line indices. The Balmer indices are consistent with the subsolar [Fe/H] observed GCs. The observed C dominated CH 4300 index is weaker and the N dominated $CN_1$ index is stronger than our solar abundance models but are broadly consistent with the C depleted, N enhanced model. The stronger Na D indices than our solar model are consistent with both GCs being Na enhanced. Both the PaT and the Na 8190 indices are affected by TiO bands and the weak observed indices are likely due to the effects of strong TiO absorption on their continuum passbands.

Downloaded from https://academic.oup.com/mnras/article-abstract/478/2/2368/4995915
by Liverpool John Moores University user
on 10 July 2018

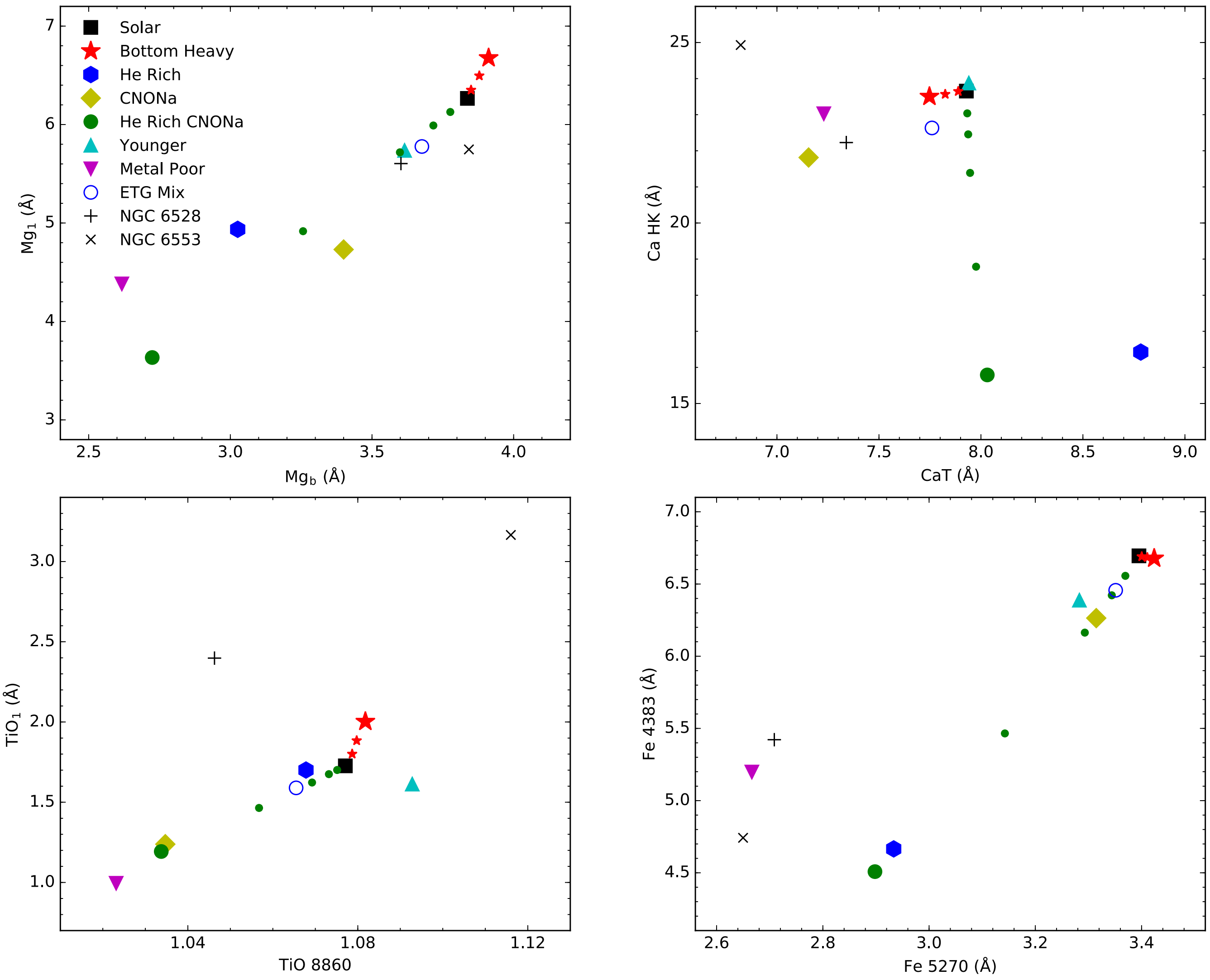

**Figure B2.** Comparison of model line index strengths with observations. The symbol shapes and colours are as in Fig. 6. *Top left:* Mg$_1$ MgH molecular band strength versus Mg$_b$ line index. *Top right:* Strength of the Ca H and K lines versus the strength of the calcium triplet (CaT). *Bottom left:* The TiO$_1$ and TiO 8860 TiO molecular indices. *Bottom right:* The Fe 4383 and Fe 5270 indices. The Mg and Fe indices are all consistent with the subsolar [Fe/H] and slightly supersolar [Mg/Fe] observed GCs. Given the large observational uncertainty on the Ca H & K lines, the models are consistent with the observations of the near solar [Ca/H] GCs. The models do not predict the observed TiO bands nor do the TiO band strengths of the two GCs agree with one another. The strong observed TiO bands weaken the observed CaT strengths.

This paper has been typeset from a TEX/LATEX file prepared by the author.

Downloaded from https://academic.oup.com/mnras/article-abstract/478/2/2368/4995915
by Liverpool John Moores University user
on 10 July 2018